




Article

Comparison of Sonodynamic Treatment Set-Ups for Cancer Cells with Organic Sonosensitizers and Nanosonosensitizers

Aleksandar Radivoievych^{1,2}, Svitlana Prylutska³, Oliver Zolk^{2,4}, Uwe Ritter⁵ , Marcus Frohme^{1,*} 
and Anna Grebinyk^{1,6} 

¹ Division Molecular Biotechnology and Functional Genomics, Technical University of Applied Sciences Wildau, Hochschulring 1, 15745 Wildau, Germany; alra9717@th-wildau.de (A.R.); anna.grebinyk@desy.de (A.G.)

² Faculty of Health Sciences, Joint Faculty of the Brandenburg University of Technology Cottbus-Senftenberg, The Brandenburg Medical School Theodor Fontane and the University of Potsdam, 14476 Potsdam, Germany; oliver.zolk@mhb-fontane.de

³ Department of Plants Physiology, Biochemistry and Bioenergetics, National University of Life and Environmental Science of Ukraine, Heroyiv Oborony Str., 15, 03041 Kyiv, Ukraine; psvit_1977@ukr.net

⁴ Institute of Clinical Pharmacology, Brandenburg Medical School, Immanuel Klinik Ruedersdorf, 15562 Ruedersdorf, Germany

⁵ Institute of Chemistry and Biotechnology, Technical University of Ilmenau, 98693 Ilmenau, Germany; uwe.ritter@tu-ilmenau.de

⁶ Deutsches Elektronen-Synchrotron DESY, Platanenallee 6, 15738 Zeuthen, Germany

* Correspondence: mfrohme@th-wildau.de; Tel.: +49-(0)-3375-508-249

Abstract: Cancer sonodynamic therapy (SDT) is the therapeutic strategy of a high-frequency ultrasound (US) combined with a special sonosensitizer that becomes cytotoxic upon US exposure. The growing number of newly discovered sonosensitizers and custom US in vitro treatment solutions push the SDT field into a need for systemic studies and reproducible in vitro experimental set-ups. In the current research, we aimed to compare two of the most used and suitable SDT in vitro set-ups—"sealed well" and "transducer in well"—in one systematic study. We assessed US pressure, intensity, and temperature distribution in wells under US irradiation. Treatment efficacy was evaluated for both set-ups towards cancer cell lines of different origins, treated with two promising sonosensitizer candidates—carbon nanoparticle C₆₀ fullerene (C₆₀) and herbal alkaloid berberine. C₆₀ was found to exhibit higher sonotoxicity toward cancer cells than berberine. The higher efficacy of sonodynamic treatment with a "transducer in well" set-up than a "sealed well" set-up underlined its promising application for SDT in vitro studies. The "transducer in well" set-up is recommended for in vitro US treatment investigations based on its US-field homogeneity and pronounced cellular effects. Moreover, SDT with C₆₀ and berberine could be exploited as a promising combinative approach for cancer treatment.

Keywords: ultrasound; C₆₀ fullerene; berberine; sonodynamic therapy; apoptosis



Citation: Radivoievych, A.; Prylutska, S.; Zolk, O.; Ritter, U.; Frohme, M.; Grebinyk, A. Comparison of Sonodynamic Treatment Set-Ups for Cancer Cells with Organic Sonosensitizers and Nanosonosensitizers. *Pharmaceutics* **2023**, *15*, 2616. <https://doi.org/10.3390/pharmaceutics15112616>

Academic Editors: Nejat Düzgüneş and Tao Yang

Received: 2 October 2023

Revised: 31 October 2023

Accepted: 7 November 2023

Published: 11 November 2023



Copyright: © 2023 by the authors. Licensee MDPI, Basel, Switzerland. This article is an open access article distributed under the terms and conditions of the Creative Commons Attribution (CC BY) license (<https://creativecommons.org/licenses/by/4.0/>).

1. Introduction

Despite technological and therapeutic advances in cancer care, the number of cancer patients is growing annually. A total of 17 million new cancer cases were diagnosed in 2016 and reached approximately 20 million in 2022, and cancer deaths increased from 9 million in 2016 to over 10 million in 2022 [1,2]. Therefore, cancer remains as the second leading cause of death worldwide [3]. Conventional strategies such as chemotherapy, surgery, and radiotherapy struggle with low target selectivity and harmful side effects [4–7]. The search for more selective and efficient methods has focused on switchable therapeutics such as sonodynamic therapy (SDT), which originated as a photodynamic therapy (PDT) branch. Unlike PDT, where visible and NIR light is used, SDT uses high frequency ultrasound (US) for a non-thermal, non-invasive, and local tumor ablation based on the toxicity induction of specific chemical sensitizers (sonosensitizers). In that way, dual tumor tissue

selectivity can be realized through the targeted accumulation of sonosensitizers in tumor tissue and the US treatment of tumor tissue. SDT can be highly selective, minimizing damage to healthy surrounding tissues and reducing side effects commonly associated with traditional therapies [8]. As a non-invasive treatment, it does not require surgical incisions or the removal of tumor tissue, resulting in reduced pain, shorter recovery time, and lower infection risk [5]. Moreover, SDT-initiated reactive oxygen species (ROS) elicit an immune response to target cancer cells [9,10]. SDT can be repeated as needed without cumulative toxicity concerns [11,12]. In addition, SDT can be used with other treatment modalities, including surgery or chemotherapy, and photodynamic, photothermal, or radiation therapy, to achieve synergistic effectiveness, offering potential multi-pronged cancer care [13]. Conventional US-based methods such as high-intensity focused ultrasound (HIFU) therapy rely on focused energy to heat and destroy cancer cells. Ensuring precise control over the extent and distribution of this heat within the tumor can be challenging and can unintentionally damage healthy tissues surrounding the tumor [6]. In addition, concerns of recurrence exist after HIFU treatment [14]. Nevertheless, the standard limitation of all US treatment methods is the difficulty in penetrating through bone and air, which can limit US treatment effectiveness towards some cancers such as osteosarcoma [15].

The principle of SDT is the sonosensitizing activity induction of particular molecules during sonication. The distribution of US waves in liquid leads to the formation of tiny vapor-filled bubbles, which cavitate and collapse. A rapid bubble implosion heats its interior and produces an intense concentration of energy that results in light emission, called sonoluminescence [16–18]. Then, sonoluminescence can induce the excitation of sensitizers. After photon absorption, the sensitizer rises to a short-lived excited state, which can be quenched by molecular oxygen to generate ROS [19,20]. Constant intensification of ROS production leads to oxidative stress and apoptosis of treated cancer cells [21,22]. Oxidative stress also causes DNA damage and induces cell cycle arrest within the cancer cell [23]. In addition, the SDT-induced ROS influence the extracellular matrix, blood vessels, and immune cell activity within the tumor [9,11]. SDT-induced ROS trigger an immune response against cancer cells. The damage caused by ROS can release tumor-associated antigens that alert the immune system to the presence of a tumor [9,10,24]. This can potentially lead to the activation of immune cells that target and destroy cancer cells.

A hematoporphyrin was found to be the first molecule to show cytotoxicity increase towards mouse sarcoma 180 and ascites hepatoma 130 cells under the action of 1.92 MHz US [18,25,26]. The sonosensitizing activity was further discovered for other organic molecules [25,27–29], as well as metal-containing [30–32] and carbon nanoparticles such as nanotubes [33,34], nanoribbons [35], and fullerenes [36–39]. Nanoparticles offer several advantages in comparison with organic molecules, including, but not limited to, improved bioavailability, smaller efficient drug doses, less toxicity, and targeting of tumor tissue [31,35,40].

The growing number of newly discovered sonosensitizers pushes the SDT field into a need for systemic studies and reproducible *in vitro* experimental set-ups. Based on the position of transducers and cell culture vessels (wells with cells), four main types of *in vitro* US set-ups were defined by Hensel et al. [41]: (1) “well on transducer”—well is placed on transducer and coupled by gel; (2) “well on water surface”—well is placed on the water surface in US bath; (3) “sealed well”—well is submerged into US bath; and (4) “Transducer in well”—transducer is directly submersed in well [41]. Table 1 summarizes the US *in vitro* set-ups for investigating metal and carbon nanoparticles as sonosensitizers towards cancer cells. If an original article lacked a US set-up description, it was excluded from Table 1.

Table 1. SDT in vitro set-ups and treatment models.

US Exposure Set-Up	Sonosensitizers	In Vitro Model	US Treatment	Year of Publication	Reference
“well on transduce”	Polypyrrole-coated carbon nanotubes	Melanoma C540	1 MHz 1.0 W/cm ² non defined	2020	[33]
	Ferrite/carbon nanocomposite	Melanoma C540	1.0 MHz 1.0 W/cm ² 60 s	2019	[30]
	Fullerene covalently bonded onto the surface of black phosphorus nanosheets	Murine breast cancer 4T1	1.0 MHz 1.0 W/cm ² 300 s	2021	[39]
	TiO ₂ conjugated to polyethylene glycol	Glioblastoma U251	1.0 MHz 1.0 W/cm ² 50 s	2011	[31]
“well, on the water’s surface”	Polyhydroxy C ₆₀	Sarcoma 180	1.92 MHz 4.5 W/cm ² 60 s	2013	[38]
	C-doped TiO ₂	Murine breast cancer 4T1	1.0 MHz 1.8 W/cm ² 90 s	2020	[32]
	C ₆₀ aqueous solution	Human cervix adenocarcinoma HeLa	1.0 MHz 5.4 W/cm ² 60 s	2023	[36]
“sealed well”	Protohemin-conjugated multiwalled carbon nanotubes with carboxylic groups	Hepatocellular carcinoma HepG-2	1.0 MHz 0.5 W/cm ² 100 s	2016	[34]
	Polyhydroxy C ₆₀	Human promyelocytic leukemia HL-60	1.93 MHz 6 W/cm ² 180 s	2016	[37]
“transducer in well”	Pegylated graphene nanoribbons conjugated with chlorin e6	Human ovarian cancer SKOV-3	1.0 MHz 0.8 W/cm ² 30 s	2011	[35]
	DEG (7,12-bis(1-(2-(2-hydroxyethoxy)ethoxy)ethyl)-3,8,13,17-tetramethylporphyrin-2,18-dipropionatomanganese)	Human lung cancers LU65A, HLC-1, KNS-62; human gastric cancers MKN-1, MKN-28, MKN-45, MKN-74; human pancreatic cancers QGP-1 MIA PaCa-2; human prostate cancer PC-3 A human liver cancer KIM-1 Human colon cancers HT-29, T-84, Caco-2; human breast cancers SK-BR-3, MCF-7	1.0 MHz 1.0 W/cm ² 120 s	2012	[29]

The “well on transducer” is often characterized by the uneven pressure distribution over the cell layer [41]. One of the main disadvantages of the “well on water surface” set-up is the possible high-temperature effect of the US due to considerable liquid–air and plastic–air interfaces that can lead to low reproducibility of results [42]. The “sealed well” is preferable for in vitro SDT experiments because of its minor US reflections and negligible temperature effects. However, to avoid any possible external effects, a well with cells must be free of air bubbles and reliably sealed [41]. The efficiency of the “transducer in well” set-up depends on its variations in the transducer distance and the thickness of a well’s bottom. Despite these variations, it is easy to implement in sterile conditions and achieves high reproducibility [41,42]. One way to overcome the negative impact of liquid–air and plastic–air interfaces for the “transducer in well” could be to position one extra water tank below the well. However, the SDT in vitro studies often lack detailed US set-up descriptions, making generated data difficult to reproduce, compare, and predict.

In the presented research, we aimed to compare two of the most commonly used SDT in vitro set-ups—“sealed well” and “transducer in well”—in one systematic study. We assessed the distribution of US pressure, intensity, and temperature in wells under US

irradiation in “sealed well” and “transducer in well” set-ups. Moreover, we studied the applicability of those set-ups for cellular effect analysis based on evaluating cell viability and caspase 3/7 activity, ROS, and ATP levels in cancer cells of different origins treated with two promising sonosensitizer candidates and 1 MHz US. The current study selected one organic (berberine) and one nanomaterial (C_{60}) sensitizer as test compounds. Natural alkaloid berberine is a promising agent for cancer chemotherapy and PDT [43]. US energy via sonoluminescence can be absorbed by berberine and C_{60} , promoting the molecule transition from its ground state to an excited state. The excited state can transfer its energy to oxygen generating ROS [44,45], which points to berberine and C_{60} as potential sonosensitizers for SDT. Other than sonosensitizing activity, berberine has proapoptotic effects by inhibiting mitochondrial respiration and modulation of signaling pathways related to cell proliferation [46]. Considerable attention is also devoted to C_{60} as a potential regulator of oxidative balance in biological systems. Low toxicity [47,48] and excellent photosensitizing activity [49,50] of C_{60} make it a promising photo- [36,49] and sonosensitizer [36]. The low photobleaching, high quantum yield, photostability, and improved biocompatibility make C_{60} a prospective molecule for cancer treatment applications [49,51,52].

2. Materials and Methods

2.1. Chemicals

Dulbecco’s modified Eagle’s medium (DMEM), Eagle’s minimum essential medium (EMEM), phosphate-buffered saline (PBS), fetal bovine serum (FBS), penicillin/streptomycin, l-glutamine, and trypsin were obtained from PAN-Biotech GmbH (Aidenbach, Germany). 3-(4,5-dimethylthiazol-2-yl)-2,5-diphenyl tetrazolium bromide (MTT) and dihydroethidium (DHE) were obtained from Biomol GmbH (Hamburg, Germany). Trypan blue and dimethylsulfoxide (DMSO) were obtained from Carl Roth GmbH + Co. KG (Karlsruhe, Germany). Berberine was obtained from Sigma-Aldrich Co. (St. Louis, MO, USA) and dissolved in sterile distilled water. Caspase-Glo[®] 3/7 Assay Systems and Mitochondrial ToxGlo[™] Assay kits were obtained from Promega GmbH (Walldorf, Germany). The pristine C_{60} aqueous colloid solution was prepared by C_{60} transfer from toluene to water using continuous ultrasound sonication [53].

2.2. Ultrasound Exposure

A vacuum pump Savant UVS 400A SpeedVac (Thermo Fisher Scientific Inc., Berlin, Germany) was used for degassing water for the US bath. Cancer cells were seeded and incubated with sonosensitizers for 24 h using cell-based assays, as described below.

2.2.1. “Sealed Well” Set-Up

A plate holder was designed and 3D-printed by Oculyze GmbH (Wildau, Germany) for positioning the 96-well plates inside the US bath. The well plate was placed 25 mm above the US transducer. Every empty well was filled with filtered water. Afterward, the plate was covered with parafilm and submerged upside down in the bath (Figure 1a). The US generator 68.101, coupled with an MH2 transducer plate mounted on a water bath (Kaijo, Tokyo, Japan), was used for US treatment. The area and the frequency of the US transducer plate were 92.6 cm² and 950 kHz (~1 MHz), respectively. The US transducer was continuously driven at 100, 150, and 200 W. To compare the two set-ups, US energy (J/cm²) was chosen as a unit of US dose. Thus, plates with cells were exposed to 60, 90, and 130 J/cm² of US dose.

2.2.2. “Transducer in Well” Set-Up

Figure 1b schematically shows the “transducer in well” set-up for the US exposure. The US therapy unit DIGI (Strive Enterprises, Yamuna Nagar, India) was driven at 1 W/cm² in continuous wave mode for 30, 60, and 90 s, equivalent to 30, 60, and 90 J/cm² of US dose. To realize the “sealed well” set-up, a tank was filled with filtered water and placed below the Petri dish.

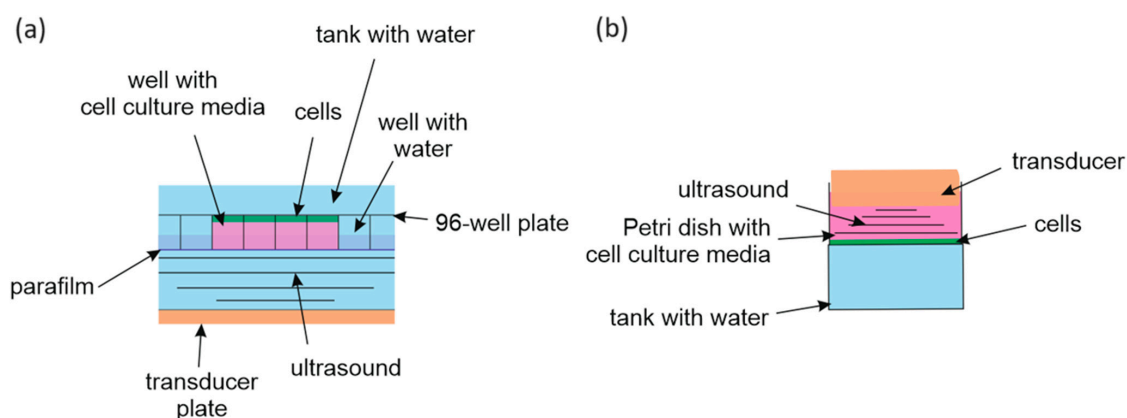


Figure 1. Diagram of the ultrasound exposure equipment: “sealed well” set-up (a); “transducer in well” set-up (b).

2.3. Sonoluminescence Detection

To detect and measure sonoluminescence, an experimental set-up was built. It consisted of the photomultiplier tube (Hamamatsu Photonics, Shizuoka, Japan), connected with the Voltcraft 6150c oscilloscope (Conrad Electronic, Hirschau, Germany) and the Thorn EMI PM28B power supply (Thorn Lighting Ltd., Spennymoor, UK). To enhance the efficiency of sonication and increase sonoluminescence intensity, the US bath was filled with degassed distilled water for better sonication and sonoluminescence intensity [54]. The wells of the plate were filled with experimental liquids: degassed distilled water, distilled water, PBS, and DMEM. Then, the filled plate was placed on the plate holder in the US bath. A polyfoam holder aligned the photomultiplier tube over one of the wells in the 24-well plate.

Sonoluminescence intensity was measured directly in the US “sealed well” set-up described above. To mimic the properties of the “transducer in well” set-up, sonoluminescence measurements were performed in the tank filled with experimental liquid, and the transducer was submersed in the filled tank. This set-up is shown schematically in Figure 2. The set-up was enclosed with aluminum foil to prevent external light from reaching the photomultiplier tube, and measurements were conducted in a dark room.

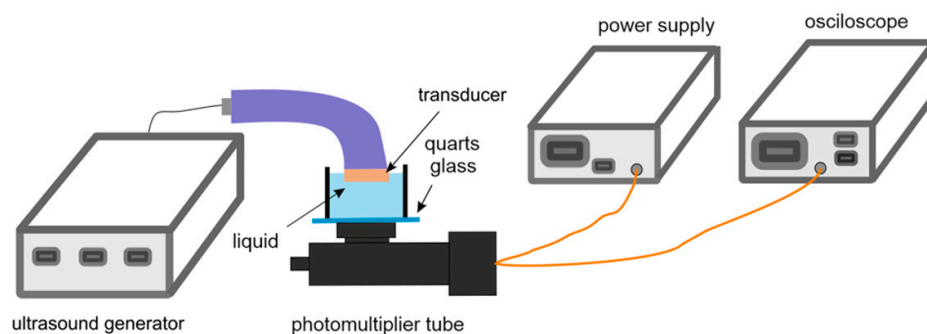


Figure 2. Diagram of the sonoluminescence “transducer in well” set-up.

The data acquired are represented as the average peak-to-peak voltage (V_{pp}) over a 120 s interval, which quantifies the complete voltage range between the positive and negative peaks in the detected voltage waveform on the photomultiplier tube.

2.4. Ultrasound Pressure and Intensity Distribution

For the measurements, a sound field scanner “AIMS III” (Onda Corporation, Sunnyvale, CA, USA), consisting of a water tank equipped with a 3-axis scanner and a “Pico-Scope 5244A” digital storage oscilloscope (DSO) (Pico Technology Limited, St Neots, UK), and an “Imotec” needle hydrophone (Imotec Montagetechnik GmbH, Hausham, Germany) incl. preamplifier (NTR) were used.

The needle hydrophone, including the preamplifier, was calibrated utilizing an “HGL-0200” calibrated capsule hydrophone (Onda Corporation, Sunnyvale, CA, USA) incl. “AH-2010” preamplifier (Onda Corporation, Sunnyvale, CA, USA). The transducers were driven by generators in continuous wave (cw) mode. Burst mode was not possible for both set-ups, and only the phase of the cw-driving signal could be used for triggering the DSO.

The hydrophone was submerged into the tank above the well plate for the “sealed well” set-up and below the well plate for the “transducer in well” set-up. The sensitive tip of the hydrophone was placed on the required positions in the sound field utilizing the 3-axis scanner. The front/back axis of the scanner was assigned to the x-direction, the left/right axis to the y-direction, and the up/down axis to the z-direction.

The following output parameters were measured at particular points in a sound field:

p+: peak compressional acoustic pressure (MPa);

p−: peak rarefactional acoustic pressure (MP);

p_{pp}: peak-to-peak acoustic pressure (MPa);

I_{ta}: temporal average intensity (W/m²) (the values of the temporal average intensity I_{ta} are calculated for an assumed cw (continuous wave) excitation by dividing the squared amplitude of the pressure wave with 2 and Z (Z = ρc, the acoustic impedance of the propagation medium water)):

$$I_{ta} = \frac{p_+^2}{2\rho c}$$

2.5. Temperature Measurement

The temperature profiles of the plates and Petri dishes were visualized with a Fluke Ti100 infrared (IR) camera (Fluke Corporation, Everett, WA, USA) after sonication in both set-ups with the parameters described above. Obtained pictures were processed and analyzed with Smart View Classic 4.4 (Fluke Corporation, Everett, WA, USA).

2.6. Cell Culture

The human cervix adenocarcinoma cell line (HeLa) was generously provided by Dr. Müller (Division of Gastroenterology, Infectiology and Rheumatology, Charité Universitätsmedizin, Berlin, Germany). The Lewis lung carcinoma cell line (LLC) was obtained from (Tebu-Bio GmbH, Offenbach, Germany). The adenocarcinoma human alveolar basal epithelial cell line (A549) and the rat hepatoma cell line (H4IIE) were obtained from Hölzel Diagnostika Handels GmbH (Cologne, Germany). HeLa, LLC, and A549 cells were maintained in DMEM. EMEM was used to maintain the H4IIE cells. Both cell culture media were supplemented with 10% FBS, 1% penicillin/streptomycin, and 2 mM glutamine. Cells were cultured in 25 cm² flasks at 37 °C with 5% CO₂ in a humidified incubator binder (Tuttlingen, Germany). A trypsin solution (1:10 in PBS) was used to detach adherent cells. The viable cells were counted upon 0.1% trypan blue staining with a Roche Cedex XS analyzer (Basel, Switzerland).

2.7. Cell Viability

Cancer cells were seeded in 96-well plates at 2×10^4 cells per well and in Petri dishes $\varnothing = 35$ mm at 1.5×10^5 cells per well (both from Sarstedt AG & Co. KG, Nümbrecht, Germany). At 24 h, cells were transferred into 1% FBS DMEM medium containing 20 μM C₆₀ or 20 μM berberine. The control cells received treatment with an equal volume of sterile water. After 24 h, treated cells were sonicated with the 1 MHz US with the respective US set-up (Figure 1). To estimate cell viability, cells were incubated for 2 h at 37 °C in the presence of 0.5 mg/mL MTT [55] 24 h after US treatment. The DMSO was used to dissolve the diformazan crystals. The absorbance was measured at 570 nm using a Tecan Infinite M200 Pro microplate reader (Tecan Trading AG, Männedorf, Switzerland). Phase contrast microscopy was carried out with the Keyence BZ-9000 BIOREVO microscope (Keyence Corporation, Osaka, Japan). Images were captured and processed with a BZ-II Viewer (Keyence Corporation, Osaka, Japan).

2.8. Intracellular Reactive Oxygen Species Generation

After US exposure, cells were trypsinized, calculated, and transported to a black 96-well plate containing 10^4 cells per well. To determine ROS production, dihydroethidium (DHE) was applied. A DHE (10 mM) stock solution was prepared in DMSO, stored at $-20\text{ }^{\circ}\text{C}$, and diluted with PBS immediately before use. Cells (10^4 /well) were treated as indicated above and washed once with PBS at 1 h and 3 h of further incubation. DHE (10 μM) was added, and the fluorescence ($\lambda_{\text{ex}} = 495\text{ nm}$, $\lambda_{\text{em}} = 585\text{ nm}$) was recorded with the Tecan Infinite M200 Pro microplate reader.

2.9. Intercellular ATP Content

Cells were treated as indicated in the cell viability section. After US exposure, cells were trypsinized, calculated, and transported to a white 96-well plate transferred in 50 μL glucose-free DMEM in a concentration of 10^4 cells per well. Then, cellular ATP levels were estimated with the mitochondrial ToxGlo™ assay kit (Promega GmbH, Walldorf, Germany) according to the manufacturer's instructions. The plates were equilibrated to room temperature for 10 min, and 50 μL of the ATP detection reagent was added to each well. The ATP detection reagent consisted of ATP detection containing luciferin, ATPase inhibitors, and thermostable luciferase. After shaking at 600 rpm for 1 min, the Tecan Infinite M200 Pro microplate reader was used to measure the luminescence intensity.

2.10. Caspase 3/7 Activity

LLC and HeLa cells were treated as described in the cell viability section. After US exposure, cells were trypsinized, calculated, and transported to a white 96-well plate containing 10^4 cells per well. The activity of caspases 3/7 was determined during a 4 h period after light exposure using the Caspase-Glo® 3/7 activity assay kit (Promega GmbH, Walldorf, Germany) according to the manufacturer's instructions. The plates were removed from the incubator and allowed to equilibrate to room temperature for 30 min. After treatment, an equal volume of Caspase-Glo 3/7 reagent was added, followed by gentle mixing with a plate shaker at 300 rpm for 1 min. The plate was then incubated at room temperature for 30 min. The luminescence of each sample was measured with the Tecan Infinite M200 Pro microplate reader.

2.11. Statistics

Each experiment was conducted with at least four replicates. Data analysis utilized GraphPad Prism 7 (GraphPad Software Inc., San Diego, CA, USA) and STATISTICA 12 (StatSoft GmbH, Hamburg, Germany). Paired Student's *t*-tests were used. The threshold for statistical significance was established at $p < 0.01$.

3. Results and Discussion

3.1. Sonoluminescence Intensity

The optical measurements were conducted using a photomultiplier tube connected to the oscilloscope to assess sonoluminescence intensity. To follow the effect of the chemical composition of the media, the sonoluminescence was measured in degassed distilled water, distilled water, phosphate buffered saline (PBS), and cell culture Dulbecco's modified Eagle medium (DMEM). The V_{pp} (peak-to-peak voltage) signal intensity value corresponded to the light reaching the photomultiplier tube. The measurements were conducted in a water bath with 0–5.4 W/cm^2 output power from the US generator ("sealed well" set-up) and 0–3 W/cm^2 output power from the US therapy unit ("transducer in well" set-up). The results were normalized using the corresponding V_{pp} measurements obtained when the shutter of the photomultiplier window was closed and the US was turned on.

The observed rise in the V_{pp} signal confirmed the presence of sonoluminescence during the propagation of 1 MHz US through liquids in both set-ups (Figure 3). In the "sealed well" set-up, the detected sonoluminescence level increased with the higher output power from the US generator in all tested media. The assessed V_{pp} evidenced the highest

sonoluminescence in the degassed distilled water. The difference in the reduced sonoluminescence level in distilled water, PBS, and DMEM was negligible. A similar tendency was observed in the tank with the submerged transducer at the “transducer in well” set-up. The results agree with our previous study [36] and correlate with other publications [56]. Dissolved gases can become trapped within the bubble during its formation. These trapped gases can affect the dynamics of the bubble’s collapse and significantly alter the conditions required for sonoluminescence to occur [57,58]. Therefore, it was shown that the sonoluminescence intensity in degassed distilled water was considerably higher than in more complex chemical buffers and media (Figure 3). The level of sonoluminescence in the “transducer in well” set-up was substantially higher than in the “sealed well” set-up. In conclusion, the detected sonoluminescence, which occurred during 1 MHz US propagation in the DMEM, can be used for cell-based assays in both set-ups.

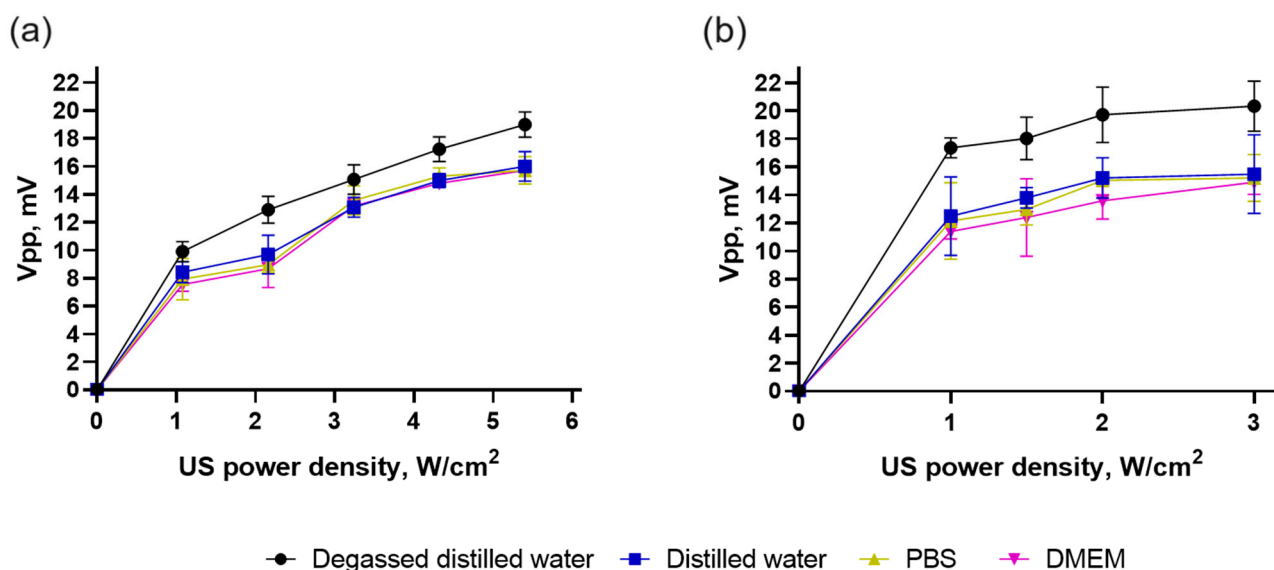


Figure 3. Sonoluminescence intensity in degassed distilled water, distilled water, phosphate buffered saline (PBS), and cell culture Dulbecco’s modified Eagle medium (DMEM): (a) in the “sealed well” set-up; (b) in the “transducer in well”.

3.2. Ultrasound Pressure and Intensity Distribution

A hydrophone converts sound vibrations into electrical energy for measurements of sound pressure and temporal average intensity; this directly describe the power and distribution of applied US energy over the well bottom. To check how the US propagated inside the cell culture vessels, sound pressure and temporal average intensity were visualized using the hydrophone in the well plate in a “sealed well” set-up and in a Petri dish in the “transducer in well”. The sound pressure and temporal intensity over the well bottom were estimated to be 1.1, 1.6, and 2.2 W/cm² for the “sealed well” set-up and 1.0 and 3.0 W/cm² of generator output power for the “transducer in well” set-up. Sound pressure and intensity increased in proportion to output power increase.

The average sound pressure and average temporal intensity over the well bottom for both set-ups were estimated and are presented in Table 2.

Table 2. Sound pressure and temporal average intensity.

Set-Up	Generator Output Power, W/cm ²	Average Sound Pressure, kPa	Average Temporal Intensity, W/cm ²
“sealed well”	1.1	179	1.1
	1.6	220	1.7
	2.2	258	2.3
“transducer in well”	1.0	450	7.0
	3.0	520	9.2

The results showed that sound pressure and temporal average intensity were higher on 271 kPa and 5.9 W/cm², respectively, in the “transducer in well” than in the “sealed well” set-up, which could be linked to a shorter distance between the transducer and well bottom—10 mm versus 25 mm, respectively. Obtained images (Figure 4) revealed uneven sound pressure and intensity distribution in a “sealed well” set-up, possibly caused by a complex well-plate structure.

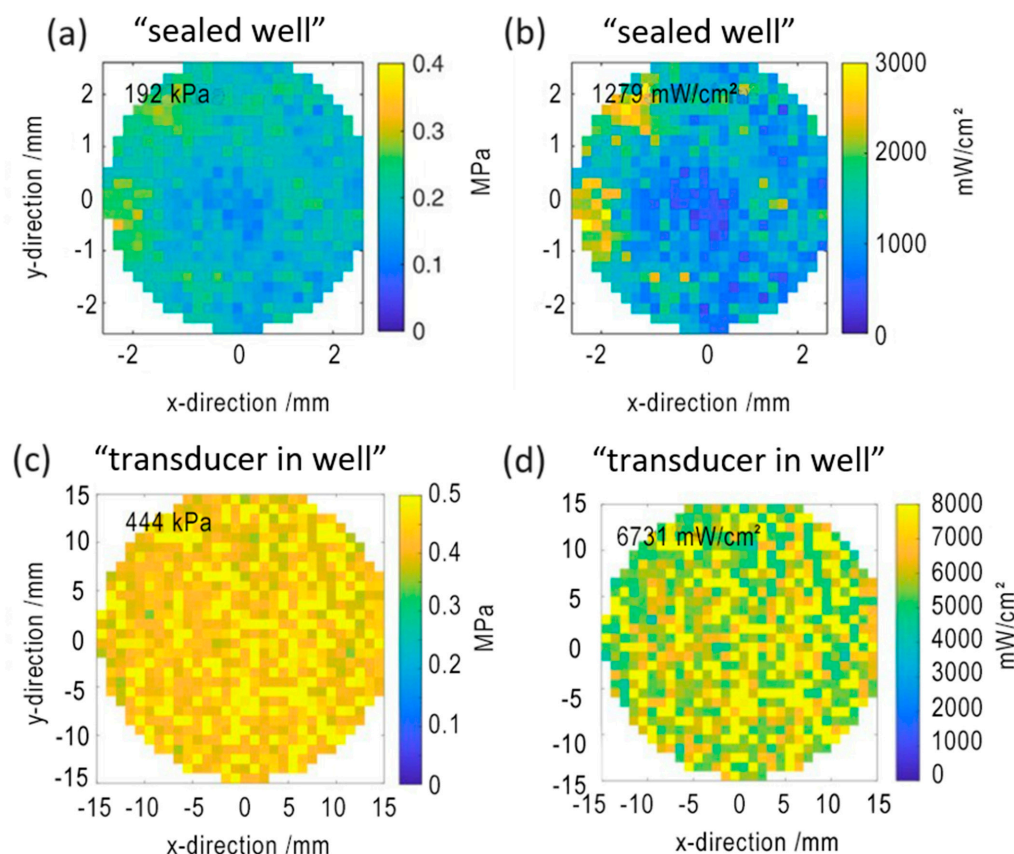


Figure 4. Temporal average intensity (a,c) and sound pressure (b,d) amplitude distribution for selected well of 96-well plate, 1 MHz transducer at 150 W, “sealed well”; for chosen Petri dish, 1 MHz transducer at 1 W/cm² “transducer in well” set-up.

Well plates and Petri dishes, common cell culture vessels for in vitro research, were selected to test “sealed well” and “transducer in well” set-ups based on transducer size. The differences in the detected US pressure and intensity distributions among set-ups pointed to better applicability of the “transducer in well” set-up due to the higher homogeneity of delivered US in the bottom of the cell culture vessel, where cells grow. On the other hand, the set-up designs made hydrophone positioning strictly at the cell-culture vessel bottom with intact bottom plastics impossible, which could introduce some uncertainties.

Moderate variation of the growth medium has a negligible effect on the sound pressure and intensity over the well bottom [41,42]. Similar measurements were performed for different set-ups [41,59,60]; however, due to varying methods of irradiation, measurement, and set-up parameters, such data are hard to compare. To increase the reproducibility of sonodynamic in vitro research, more common parameters such as US frequency (Hz), power units (W/cm^2), propagation mode, duty cycle (%), pressure, and intensity distribution, distance between transducer and well bottom (mm), should be defined.

3.3. Temperature Estimation

US energy can be converted into temperature through acoustic heating. The absorbed energy increases the kinetic energy of the particles, leading to an overall temperature rise in the liquid [61,62]. If the temperature exceeds $37\text{ }^\circ\text{C}$, cells undergo destructive changes. Therefore, the IR camera was used to exclude the possible thermal effect of the US. IR thermography images of the plate and Petri dish, filled with distilled water, and exposed to 1 MHz US in “sealed well” and “transducer in well” set-ups are shown in Figure 5a,b, correspondingly. The temperature increase during cell culture vessel exposure to the US was found in both set-ups. The detected maximum temperature in both set-ups did not exceed $36.8\text{ }^\circ\text{C}$ after $120\text{ J}/\text{cm}^2$ sonication, which indicates both set-ups’ applicability for cell-based experiments. The wells in the homogenous temperature distribution were selected for further studies with a “sealed well” set-up.

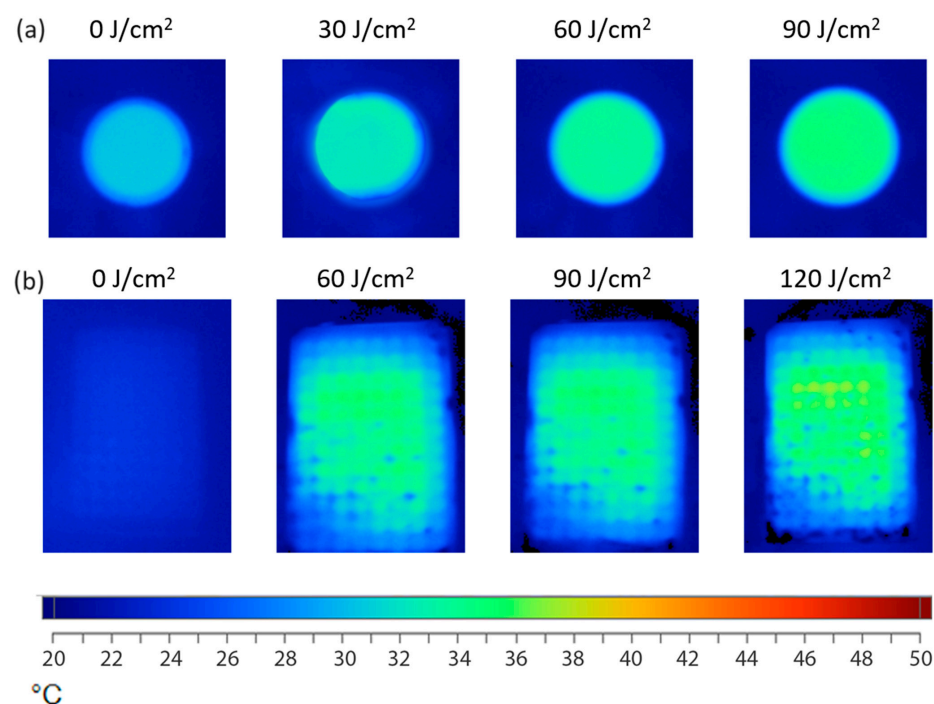


Figure 5. IR-thermography images of the Petri dish after sonication in “transducer in well” set-up (a) and the plates after sonication in “sealed well” set-up (b).

The temperature distribution in the Petri dish was even, whereas, in the 96-well plate, inhomogeneity was observed. Uneven temperature distribution could result from the well plate’s more complex plastic design. Other studies have shown that temperature insignificantly increased by only $2\text{--}3\text{ }^\circ\text{C}$ and did not rise above $37\text{ }^\circ\text{C}$ during the sonication of cells in different US set-ups [63–65]. The critical requirement of cell-based research was met, with demonstrated temperatures kept below $37\text{ }^\circ\text{C}$.

3.4. Cell Viability

Cell cultures retain the basic properties of the tumors from which they are derived. Thus, different cell lines have unique parameters of metabolism, gene expression, sensitivity,

and treatment resistance, making them integral to in vitro cancer research models. HeLa, LLC, A549, and H4IIE were chosen as cell lines of different origins. HeLa and A549 originated from human tissue, while LLC and H4IIE from mice and rats. HeLa cells are a standard model because this cell line has been pivotal in numerous scientific discoveries [66]. A549 cells are characterized by strong resistance to oxidative stress [67,68]. Meanwhile, LLC cells are tumorigenic and characterized by rapid proliferation [69]. H4IIE cells often metastasize to the lungs, bones, and regional lymph nodes [70].

To follow how physical characteristics of tested in vitro US treatment set-ups manifest in their efficiency for sonodynamic treatment of cancer cells, the toxic effects towards LLC, HeLa, H4IIE, and A549 cells were evaluated in both set-ups after incubation with C₆₀ or berberine. First, cells were treated with either 20 μ M C₆₀ or 20 μ M berberine for 24 h and then were exposed to 1 MHz US at 0–120 and 0–90 J/cm² for the “sealed well” and “transducer in well” set-ups, respectively. Then, 24 h after US exposure, cell viability was estimated with MTT assay. The viability of the respective control cells without any sonosensitizer and US treatment was considered 100%.

The viability analysis is presented for cancer cells treated in the US presence of sonosensitizers using “sealed well” and “transducer in well” set-ups in Figures 6 and 7, respectively. Control cells were incubated with equal sterile water and had no significant viability changes after sonication with low and middle doses. However, the highest US doses above 90 J/cm², which were applied in the experiments, decreased cell viability in both set-ups to $\geq 67 \pm 6\%$. US cytotoxicity depends on the specific parameters of the US exposure, including intensity, frequency, duration, and mode of operation. US-induced streaming of surrounding liquid and cavitation can directly damage cell membranes, leading to cytotoxic effects [71,72].

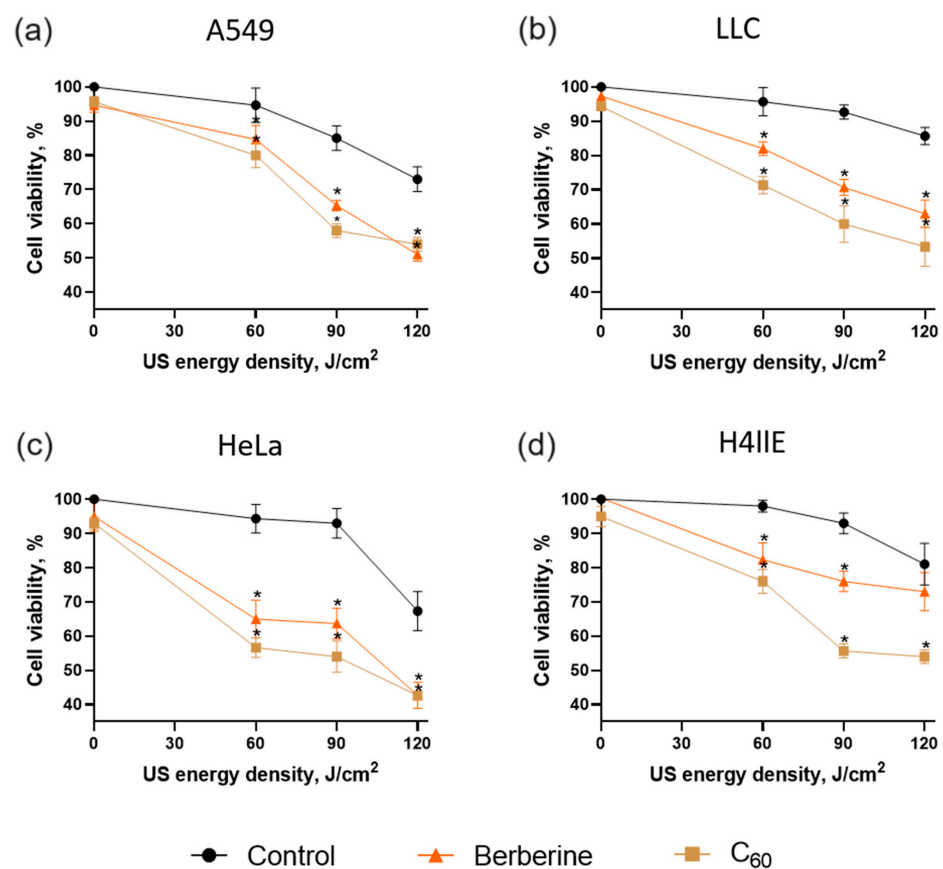


Figure 6. Viability of A549 (a), LLC (b), HeLa (c), and H4IIE (d) cells incubated in the presence of 20 μ M C₆₀ or 20 μ M berberine and treated with 1 MHz ultrasound (US) in the “sealed well” set-up; *— $p \leq 0.01$ in comparison with the viability of cells, treated with the respective duration of US.

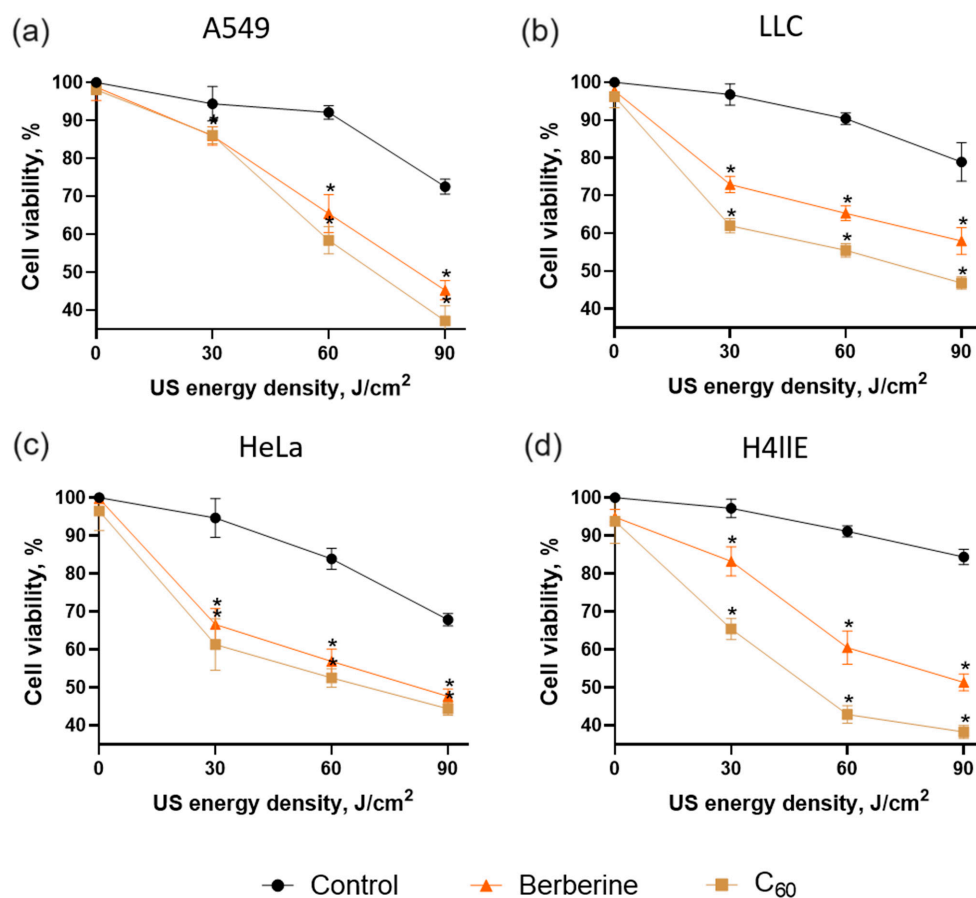


Figure 7. Viability of A549 (a), LLC (b), HeLa (c), and H4IIE (d) cells incubated in the presence of 20 μM C₆₀ or 20 μM berberine and treated with 1 MHz ultrasound (US) in the “transducer in well” set-up; *— $p \leq 0.01$ in comparison with the viability of cells, treated with the respective duration of US.

All cell lines treated with tested sonosensitizers and US demonstrated a significant decrease in cell viability (Figures 6 and 7). The highest ratio between the control and cells incubated with sonosensitizer was observed after sonication with a middle dose of US (90 and 60 J/cm² in “sealed well” and “transducer in well” set-ups, respectively). Thus, the US dose of 90 J/cm² in the presence of 20 μM C₆₀ decreased the cell viability to 58 \pm 2%, 60 \pm 6%, 54 \pm 4%, and 56 \pm 2% for A549, LLC, HeLa, and H4IIE cells, respectively, in the “sealed well” set-up. Meanwhile, berberine decreased the cell viability of A549, LLC, HeLa, and H4IIE cells to 65 \pm 2%, 70 \pm 2%, 64 \pm 4%, and 76 \pm 3%, respectively, exposed to US in the same set-up (Figure 6).

The “transducer in well” set-up demonstrated a more efficient decrease in cancer cell viability in combination with sonosensitizers at lower US power. Thus, A549, LLC, HeLa, and H4IIE cell viability was decreased to 59 \pm 3%, 56 \pm 2%, 52 \pm 2%, and 47 \pm 2%, respectively, with the US dose of 60 J/cm² in the presence of 20 μM C₆₀, while sonicated berberine in the “transducer in well” set-up decreased cell viability to 65 \pm 5%, 65 \pm 2%, 57 \pm 2%, and 60 \pm 4% for A549, LLC, HeLa, and H4IIE cells, respectively (Figure 7). In addition, morphological changes such as decreased cell density and apoptotic bodies were observed with phase contrast microscopy after treatment with sonosensitizers and 60 J/cm² US, whereas 60 J/cm² US without sonosensitizer did not affect cells (Figure 8).

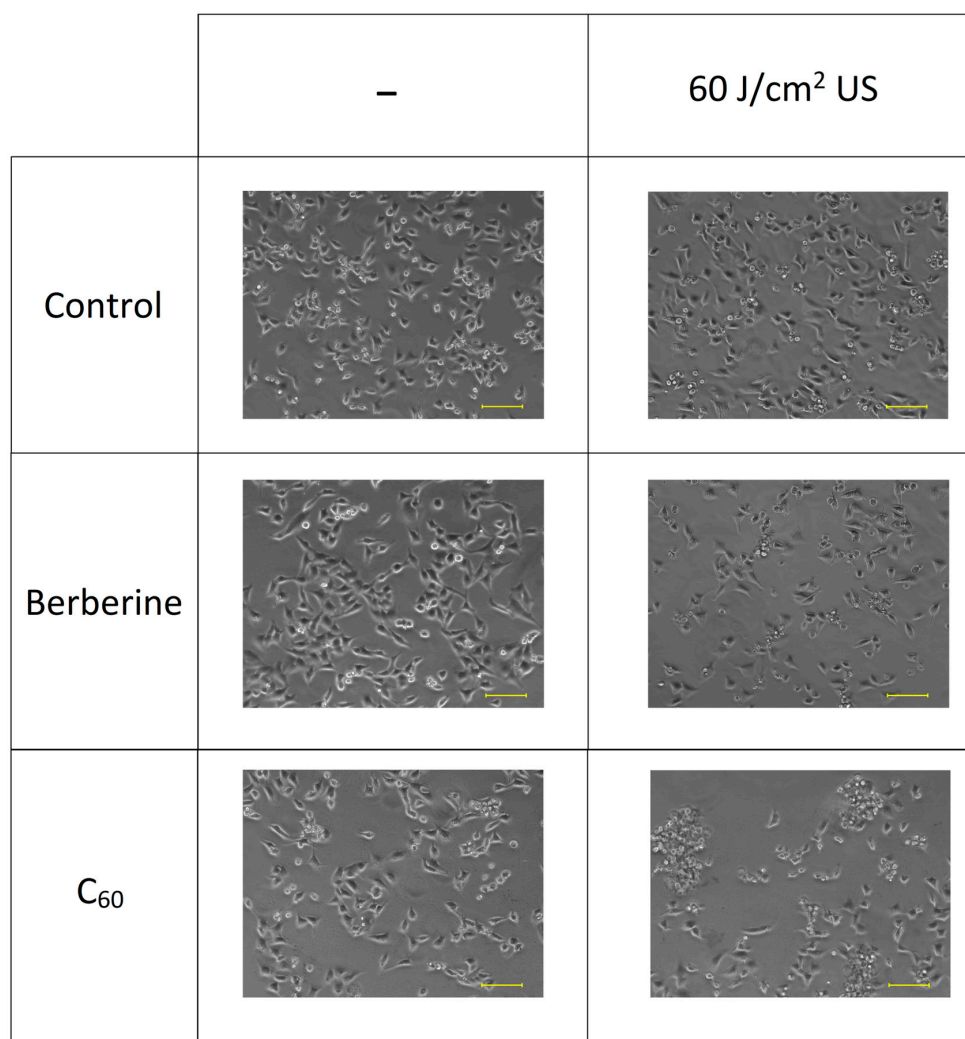


Figure 8. Phase contrast microscopy images of HeLa cells incubated in the presence of 20 μM C_{60} or 20 μM berberine and treated with 1 MHz ultrasound (US) in the “transducer in well” set-up; scale bar is 100 μm .

Cells exposed to a combined treatment of 1 MHz US and 20 μM sonosensitizers demonstrated a considerable viability decrease. C_{60} showed higher sonocytotoxicity against all tested cell lines than berberine. In addition, HeLa and H4IIE cells had higher sensitivity to treatment with C_{60} and berberine than other cell lines. Nevertheless, the “transducer in well” set-up demonstrated a higher cytotoxic effect towards A549, LLC, HeLa, and H4IIE cells treated with C_{60} and 60 J/cm² by 6%, 9%, 5%, and 13%, respectively, than the “sealed well” set-up. HeLa demonstrated higher sensitivity to the proposed treatment among human cell lines. Meanwhile, lung cancer is the leading cause of death among other types of tumor disease, and LLC has demonstrated significant sensitivity to sonodynamic treatment [2]. Therefore, LLC and HeLa cells were selected for comparison of intracellular effects as carcinoma models of different origins.

The data revealed C_{60} 's and berberine's ability to decrease cancer cell viability after sonoexcitation with 1 MHz US in both set-ups. Meanwhile, C_{60} demonstrated higher cell viability inhibition than berberine under US action. The obtained treatment cytotoxicity tendencies correlated with sonoluminescence intensity data at tested US exposure set-ups (Figures 6 and 7). The US dose increased results in higher sonoluminescence intensity and cytotoxic effect towards treated cells, suggesting the sonoluminescence-dependent induction of sonosensitizer's cytotoxicity. The spectrum of sonoluminescence consists of emission at 280, 310, and 340 nm [73,74]. C_{60} has three intense absorption bands, with

maxima around 215, 265, and 350 nm [49,53]. Meanwhile, the absorption spectrum of berberine exhibits three bands, with maxima around 250, 350, and 420 nm [43,75]. The sonoluminescence spectrum matches the first long-waved maxima of C₆₀ in a broader range than berberine, suggesting that it could induce the cytotoxic photosensitizing activity of C₆₀ more efficiently. US without sonosensitizers showed no significant cytotoxic effect on cells at a dose ≤ 60 J/cm². The highest ratio of cell viability between treated cells and corresponding control was observed at 60 J/cm² in both set-ups. The “transducer in well” set-up demonstrated higher efficacy at 6–13% for A549, LLC, HeLa, and H4IIE cells than the “sealed well” set-up. It was consistent with the US pressure and intensity distribution data, which showed higher sound pressure and temporal average intensity in the “transducer in well” than in the “sealed well” set-up.

The obtained results evidenced that 1 MHz US induced significant cytotoxic effects of proposed sonosensitizers against cancer cells. The inhibition of cell viability underlined the potential for the application of the proposed US set-ups to test sonosensitizing candidates for anticancer therapy. Similar experiments were performed by Tsuru et al., using a “transducer in well” set-up. Sixteen cell lines were treated with 7,12-bis(1-(2-(2-hydroxyethoxy)ethoxy)ethyl)-3,8,13,17-tetramethylporphyrin-2,18-dipropionatomanganese (DEG) and 1 MHz 1 W/cm² US for 120 s. As a result, the cytotoxic effect varied from 52% to 87% [29]. Meanwhile, after 180 s of 1.93 MHz 6 W/cm² US sonication in a “sealed well” set-up, the cell viability of human promyelocytic leukemia HL-60 treated with polyhydroxy C₆₀ decreased to 56% [37]. Because of minor reflections and no undesired parameter variations, the “sealed well” set-up was one of the preferable US therapy set-ups for in vitro application [41].

Meanwhile, the main advantages of the “transducer in well” set-up include ease of positioning the transducer directly in the well and reduced wave reflections [42]. Lee et al. used human ovarian cancer SKOV-3 spheroids adhered to LP-9 normal mesothelial cell monolayers and treated them with pegylated graphene nanoribbons conjugated with chlorin e6. After 30 s of 1 MHz 0.8 W/cm² US irradiation, complete cell death of SKOV-3 spheroids was detected, while LP-9 cells were not significantly affected after US irradiation [35]. Using a “transducer in well” set-up, Lee et al. showed many significant effects with less US output power than Yumita et al. showed with a “sealed well” set-up. However, comparing the research is complicated due to different models, cell lines, and sonosensitizers. Although (for experiments with a “transducer in well” set-up) sterile conditions such as a laminar flow box are required, a “transducer in well” set-up can be easily standardized and more reproducible in comparison to a “sealed well” set-up [42].

The “transducer in well” set-up can demonstrate higher efficacy and reproducibility than the “sealed well” set-up. The US therapy unit provides a user-friendly cost-effective treatment strategy for translational research with animal models, as in the “transducer in well” set-up. Transducers of the US therapy unit could be aimed at the tumor location during the treatment procedure. Therefore, the “transducer in well” set-up was chosen to estimate apoptosis cell-death type induction.

3.5. Apoptosis Induction

To estimate further cellular effects, LLC and HeLa cells were incubated with 20 μ M C₆₀ or 20 μ M berberine for 24 h, then irradiated with 1 MHz, 1 W/cm² US for 30, 60, and 90 s in the “transducer in well” set-up.

The efficient and continuous intracellular ROS production is critical for realizing the sonosensitizer’s anticancer effect [35–37,49]. Therefore, ROS generation was estimated with the ROS-sensitive fluorescence dye DHE. The ROS production was estimated 2 h after US exposure. The US irradiation insignificantly affected ROS levels in treated HeLa and LLC cells (Figure 9). After sonoexcitation of cells treated with 60 J/cm² US and C₆₀, ROS levels reached $307 \pm 20\%$ and $158 \pm 22\%$ in HeLa and LLC cells, correspondingly. Berberine demonstrated lower ROS generation, with $134 \pm 14\%$ and $130 \pm 11\%$ ROS level increases in HeLa and LLC cells, respectively.

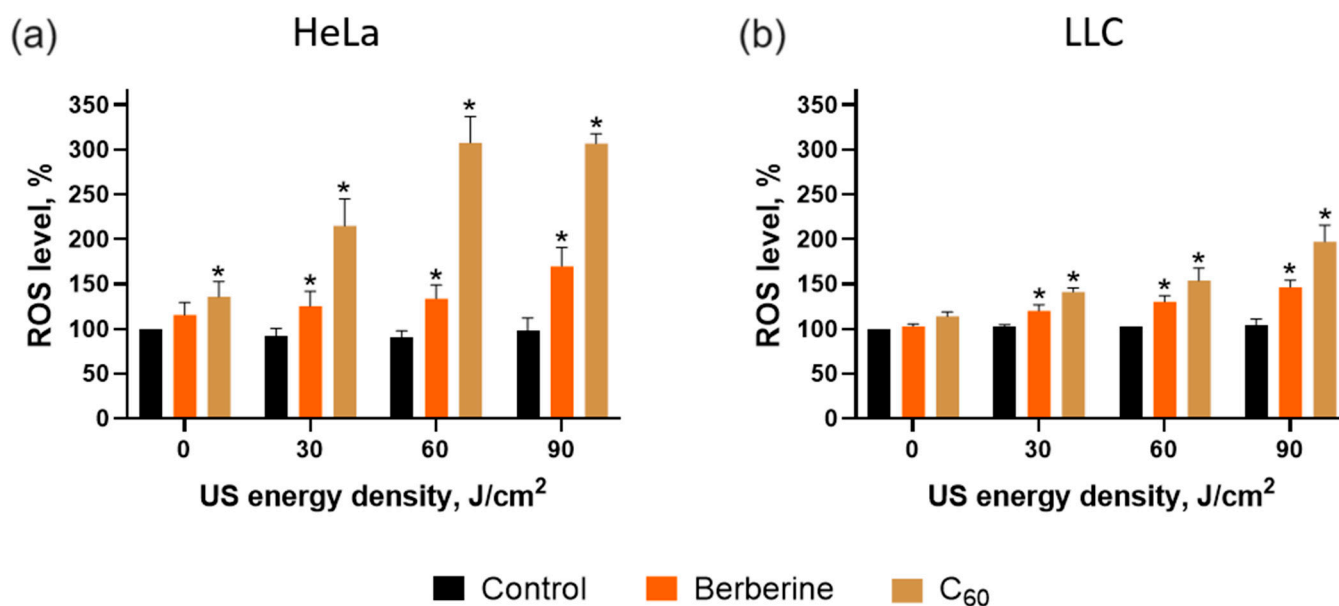


Figure 9. ROS level of HeLa (a) and LLC (b) cells incubated in the presence of 20 μM C₆₀ or 20 μM berberine and treated with 1 MHz ultrasound (US) in the “transducer in well” set-up; *— $p \leq 0.01$ in comparison with the viability of cells, treated with the respective duration of US.

ROS level measurements revealed higher sonodynamic treatment efficacy toward HeLa cells, as the ROS level of LLC cells was lower by 173% and 28% for US with C₆₀ and berberine, respectively. The obtained data can be linked to increased activity of the antioxidant system in lung cells related to the nuclear factor erythroid 2-related factor 2 (NRF2) [67,68,76].

ROS level increase leads to the loss of mitochondrial membrane integrity and cytochrome c release for further apoptosome formation. In comparison, apoptosome is an Apaf-1-containing complex that catalyzes the activation of caspases 3/7 [77]. Therefore, the ATP level and caspase 3/7 activity were investigated as markers of apoptotic cell death.

The ATP level was assessed as a principal marker of mitochondrial activity. The ATP level was measured 4 h after US treatment. Neither C₆₀, berberine, nor US affected the ATP level in the cancer cells. In contrast, the sonication at 60 J/cm² of HeLa and LLC cells treated with 20 μM C₆₀ caused a decrease in the ATP level to $44 \pm 2\%$ and $26 \pm 1\%$, respectively (Figure 10). Meanwhile, berberine induced the ATP level to drop to $55 \pm 5\%$ and $38 \pm 5\%$ in HeLa and LLC cells, respectively, after sonication at 60 J/cm².

The decrease in ATP levels evidenced the mitochondrial toxicity of the sonodynamic treatment of cancer cells. As apoptosis is an ATP-dependent process, a lack of ATP could lead to unprogrammed necrotic cell death and an inflammatory process. Apoptosis is the most favorable process of programmed, ATP-dependent, and autonomous cellular dismantling that avoids eliciting inflammation [77,78]. Therefore, as a total ATP drop was not evidenced, apoptotic cell death could be executed.

Activated caspase 3/7 executes apoptosis [77]. Therefore, the proapoptotic ability of the combinative treatment of C₆₀ and berberine with 1 MHz, 1 W/cm² US towards cancer cells was studied by evaluating the caspase 3/7 activity as a primary marker of apoptosis. Caspase 3/7 activity in treated cancer cells was estimated 4 h after sonication with 1 MHz, 1 W/cm² US. It was shown that US did not affect caspase 3/7 activity. Meanwhile, the sonodynamic treatment with C₆₀ and 60 J/cm² US increased caspase 3/7 activity to $326 \pm 23\%$ and $307 \pm 24\%$ in HeLa and LLC cells, respectively (Figure 11). Berberine demonstrated lower caspase 3/7 activity induction under US action, reaching $136 \pm 12\%$ and $138 \pm 18\%$ in HeLa and LLC cells, respectively.

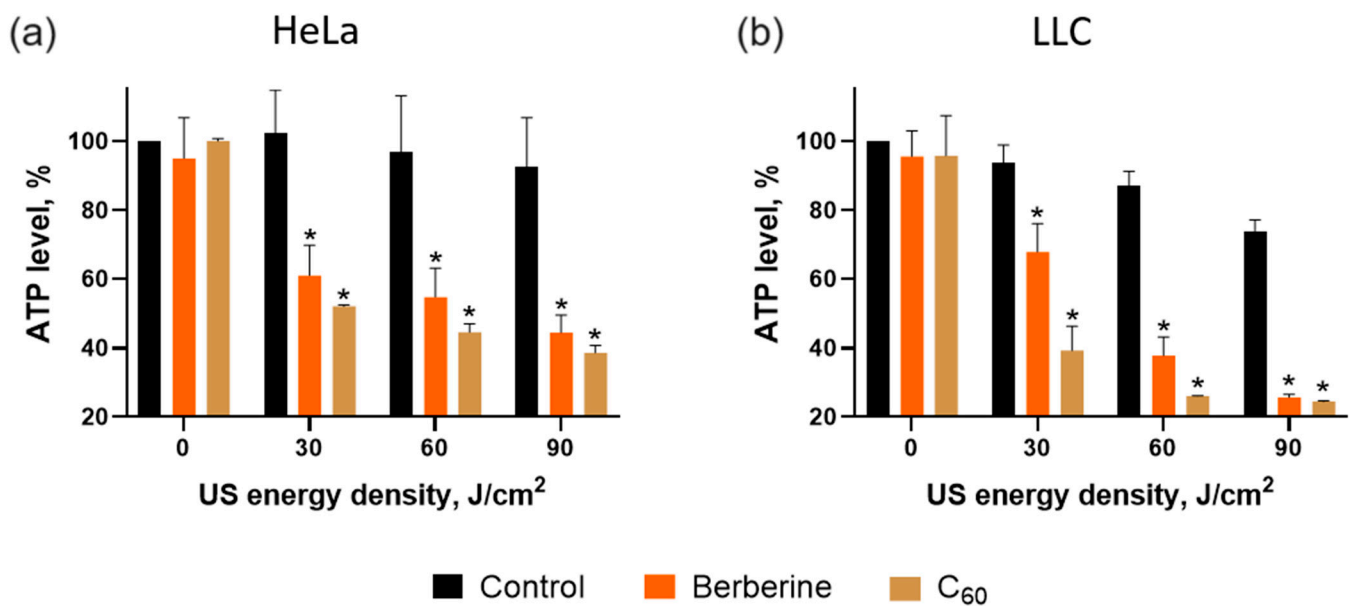


Figure 10. ATP level of HeLa (a) and LLC (b) cells incubated in the presence of 20 μ M C₆₀ or 20 μ M berberine and treated with 1 MHz ultrasound (US) in the “transducer in well” set-up; *— $p \leq 0.01$ in comparison with the viability of cells, treated with the respective duration of US.

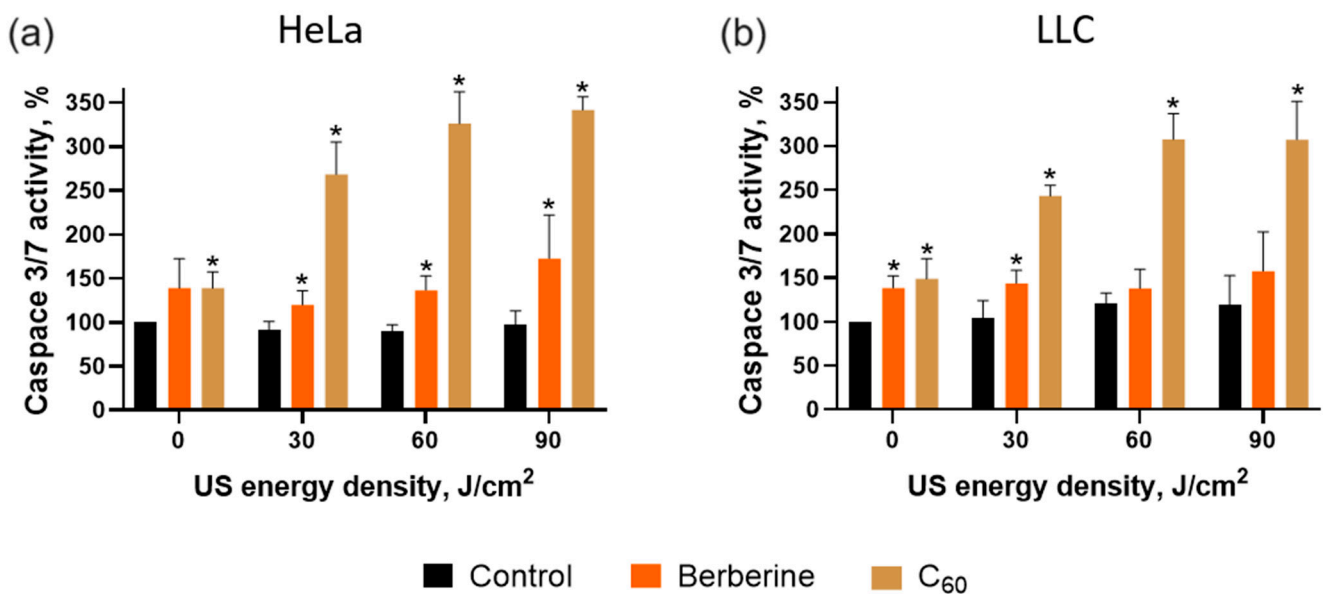


Figure 11. Caspase 3/7 activity of HeLa (a) and LLC (b) cells incubated in the presence of 20 μ M C₆₀ or 20 μ M berberine and treated with 1 MHz ultrasound (US) using “transducer in well” set-up; *— $p \leq 0.01$ in comparison with the viability of cells, treated with the respective duration of US.

Since the employment of fullerenes, as well as SDT itself, for cancer treatment is still at the early stages of development, high attention should be paid to an identification of its possible toxicity and safety.

Our previous studies were focused on the evaluation of possible effects of C₆₀ aqueous colloid solution on normal cells such as human primary keratinocytes hMSC cells, nondifferentiated rat pheochromocytoma PC-12 neuronallike cells, normal human mammary epithelial MCF10A cells, baby hamster kidney BHK-21 cells, and human embryonic kidney HEK293 cells. Thus, Tolkachov M. et al. showed that 6, 12, 18, and 24 μ g/mL C₆₀ did not affect the cell viability of hMSC cells for up to 24 h of incubation [79]. Prylutska S. et al. described the

absence of the cytotoxic activity of C₆₀ in a concentration range of 3.6–144 mg/mL against HEK293 cells at 24 h [80]. In addition, toxicity against MCF10A, PC-12, hMSC, and BHK-21 cells were described by Levi N. et al., Larner S. et al., Scrivens W. et al., and Liu S. et al., accordingly [81–84]. Summarizing the literature and our previous data, we conclude that the proposed pristine C₆₀ aqueous colloid solution could be defined as nontoxic at the used concentrations towards normal cells.

Concerning the herbal alkaloid berberine, safety concerns should be evaluated as well. Published articles report that the safe dose of berberine in vivo for oral administration in mice is 20.8 g/kg of body weight, while intravenously it is 0.38 µg/mL [85]. Cytotoxic concentration of berberine towards normal cells varies from 47 to 293 µM [86], which is at least two times more than the used concentration in this research (20 µM), suggesting its applicability.

Several studies have reported SDT to be safe for normal cells and tissues. Lagneaux et al. showed that leukemia cells were damaged by 1.8 MHz 0.22 W/cm² US, while normal hematopoietic cells remained unaffected [87]. Other published data reporting that US had no effect towards normal endothelial cell lines, while tumor cells were significantly affected [88]. Ohmura et al. demonstrated that the normal rat brain tissue was unaffected under long-term US with an intensity of 10 W/cm² [89].

Our previous research evidenced the selective toxicity of C₆₀-based SDT towards cancer cells. The treatment of normal human embryonic lung HEL 299 cells with 1 MHz US in the presence of C₆₀ led to no significant decrease in the cells' viability. Meanwhile, 60 s US treatment of HeLa cells in the presence of 20 µM C₆₀ decreased cell viability to 59 ± 5% [36]. Also, US (1.86 MHz, 1.5 W/cm², 300 s) treatment with porphyrinato palladium tetrachloride had no effect on the viability of human primary dermal fibroblast HDF 106-05 cells, while it led to a dramatic decrease in human colon cancer cell HT-29 viability [90]. Lee et al. demonstrated significant toxicity of SDT with pegylated graphene nanoribbons conjugated with chlorin e6 towards human ovarian cancer SKOV-3 spheroids. Meanwhile, an LP-9 normal mesothelial cell monolayer was not significantly affected after similar SDT treatment [35]. Therefore, we can assume that STD with sonosensitizers has selective toxicity against cancer cells, whereas the effect on normal cells is expected to be negligible.

The potential for using fullerene- or herbal alkaloid-based sonosensitizers in cancer SDT treatment protocols is substantial. Promising studies that have emerged in the last years have tested its validity and safety. The pharmacodynamics and pharmacokinetics of any new drug formulation should certainly be defined both in vitro and in vivo for an effective assessment of possible human health risks. Further research on the safety profile and treatment efficacy of the proposed treatment is ongoing.

4. Conclusions

The obtained data evidenced a toxicity of the tested sonodynamic treatment of LLC and HeLa cells with 1 MHz US and C₆₀ or berberine via oxidative stress and apoptosis induction. Combining 1 W/cm² US with C₆₀ and berberine provided a promising platform for a synergetic approach to cancer treatment. Obtained data on ROS and ATP levels and caspase 3/7 activity underlined a suitable application of the “transducer in well” set-up for sonodynamic cancer therapy evaluation in vitro and pointed to the perspective of its application for further cancer SDT development.

Author Contributions: Conceptualization, A.R., M.F. and A.G.; data curation, S.P. and A.G.; formal analysis, A.R. and A.G.; funding acquisition, A.R., U.R. and M.F.; investigation, A.R. and A.G.; methodology, A.R. and A.G.; project administration, M.F. and A.G.; resources, S.P., U.R. and M.F.; supervision, O.Z., M.F. and A.G.; validation, A.R. and M.F.; visualization, A.R. and A.G.; writing—original draft, A.R., M.F. and A.G.; writing—review and editing, S.P., U.R. and O.Z. All authors have read and agreed to the published version of the manuscript.

Funding: We thank the German Academic Exchange Service (DAAD) for their support (scholarship AR 91775672) and the Brandenburg program “Strengthening technological and application-oriented research at scientific institutions (StaF Directive)” (FullDrug, 85037298).

Institutional Review Board Statement: Not applicable.

Informed Consent Statement: Not applicable.

Data Availability Statement: The datasets used and analyzed during the current study are available from the corresponding author upon reasonable request.

Acknowledgments: We express our deep gratitude to Michael Danese from Kaijo Shibuya America Inc. (Santa Clara, CA, USA) for the generous gift of both the ultrasound transducer and generator and to Yumiko Iwasaki for the organization of its shipment. We thank Klaus-Vitold Jenderka (Hochschule Merseburg, Germany) for measuring sound pressure and intensity distribution on the bottom of the wells for two different set-ups and Sanjana Pal for final proofreading of this manuscript. We acknowledge support by the Open Access Publication Fund of Technical University of Applied Sciences Wildau.

Conflicts of Interest: The authors declare no conflict of interest. The funders had no role in the study’s design, in the collection, analyses, or interpretation of data, in the writing of the manuscript, or in the decision to publish the results.

References

1. Global Burden of Disease Cancer Collaboration. Global, Regional, and National Cancer Incidence, Mortality, Years of Life Lost, Years Lived with Disability, and Disability-Adjusted Life-Years for 29 Cancer Groups, 1990 to 2016: A Systematic Analysis for the Global Burden of Disease Study. *JAMA Oncol.* **2018**, *4*, 1553–1568. [[CrossRef](#)] [[PubMed](#)]
2. Chhikara, B.S.; Parang, K. Global Cancer Statistics 2022: The Trends Projection Analysis. *Chem. Biol. Lett.* **2023**, *10*, 451.
3. Vlad, I.; Gordon-Dseagu, V. *Differences in Cancer Incidence and Mortality across the Globe*; WCRF International: London, UK, 2023.
4. Muhamad, N.; Plengsuriyakarn, T.; Na-Bangchang, K. Application of Active Targeting Nanoparticle Delivery System for Chemotherapeutic Drugs and Traditional/Herbal Medicines in Cancer Therapy: A Systematic Review. *Int. J. Nanomed.* **2018**, *13*, 3921–3935. [[CrossRef](#)] [[PubMed](#)]
5. Nowak, K.M.; Schwartz, M.R.; Breza, V.R.; Price, R.J. Sonodynamic Therapy: Rapid Progress and New Opportunities for Non-Invasive Tumor Cell Killing with Sound. *Cancer Lett.* **2022**, *532*, 215592. [[CrossRef](#)] [[PubMed](#)]
6. Coon, J.; Todd, N.; Roemer, R. HIFU Treatment Time Reduction through Heating Approach Optimisation. *Int. J. Hyperth.* **2012**, *28*, 799–820. [[CrossRef](#)] [[PubMed](#)]
7. Zhi, D.; Yang, T.; O’Hagan, J.; Zhang, S.; Donnelly, R.F. Photothermal Therapy. *J. Control. Release* **2020**, *325*, 52–71. [[CrossRef](#)] [[PubMed](#)]
8. Xing, X.; Zhao, S.; Xu, T.; Huang, L.; Zhang, Y.; Lan, M.; Lin, C.; Zheng, X.; Wang, P. Advances and Perspectives in Organic Sonosensitizers for Sonodynamic Therapy. *Coord. Chem. Rev.* **2021**, *445*, 214087. [[CrossRef](#)]
9. Li, J.; Yue, Z.; Tang, M.; Wang, W.; Sun, Y.; Sun, T.; Chen, C. Strategies to Reverse Hypoxic Tumor Microenvironment for Enhanced Sonodynamic Therapy. *Adv. Healthc. Mater.* **2023**, *27*, 2302028. [[CrossRef](#)]
10. Chen, X.; Song, M.; Zhang, B.; Zhang, Y. Reactive Oxygen Species Regulate T Cell Immune Response in the Tumor Microenvironment. *Oxidative Med. Cell. Longev.* **2016**, *2016*, e1580967. [[CrossRef](#)]
11. Li, X.; Geng, X.; Chen, Z.; Yuan, Z. Recent Advances in Glioma Microenvironment-Response Nanoplatforams for Phototherapy and Sonotherapy. *Pharmacol. Res.* **2022**, *179*, 106218. [[CrossRef](#)]
12. Hirschberg, H.; Madsen, S.J. Synergistic Efficacy of Ultrasound, Sonosensitizers and Chemotherapy: A Review. *Ther. Deliv.* **2017**, *8*, 331–342. [[CrossRef](#)] [[PubMed](#)]
13. Xu, M.; Zhou, L.; Zheng, L.; Zhou, Q.; Liu, K.; Mao, Y.; Song, S. Sonodynamic Therapy-Derived Multimodal Synergistic Cancer Therapy. *Cancer Lett.* **2021**, *497*, 229–242. [[CrossRef](#)] [[PubMed](#)]
14. Hsiao, Y.-H.; Kuo, S.-J.; Tsai, H.-D.; Chou, M.-C.; Yeh, G.-P. Clinical Application of High-Intensity Focused Ultrasound in Cancer Therapy. *J. Cancer* **2016**, *7*, 225–231. [[CrossRef](#)] [[PubMed](#)]
15. Langton, C.M.; Njeh, C.F. Sound-Tissue Interaction: The Physical Basis of Bone Ultrasonometry and Limitations of Existing Methods. *J. Clin. Densitom.* **1998**, *1*, 295–301. [[CrossRef](#)] [[PubMed](#)]
16. Canaparo, R.; Foglietta, F.; Barbero, N.; Serpe, L. The Promising Interplay between Sonodynamic Therapy and Nanomedicine. *Adv. Drug Deliv. Rev.* **2022**, *189*, 114495. [[CrossRef](#)] [[PubMed](#)]
17. Choi, V.; Rajora, M.A.; Zheng, G. Activating Drugs with Sound: Mechanisms Behind Sonodynamic Therapy and the Role of Nanomedicine. *Bioconjugate Chem.* **2020**, *31*, 967–989. [[CrossRef](#)] [[PubMed](#)]
18. Kuroki, M.; Hachimine, K.; Abe, H.; Shibaguchi, H.; Kuroki, M.; Maekawa, S.-I.; Yanagisawa, J.; Kinugasa, T.; Tanaka, T.; Yamashita, Y. Sonodynamic Therapy of Cancer Using Novel Sonosensitizers. *Anticancer Res.* **2007**, *27*, 3673–3677.

19. Hamblin, M.R. Fullerenes as Photosensitizers in Photodynamic Therapy: Pros and Cons. *Photochem. Photobiol. Sci.* **2018**, *17*, 1515–1533. [[CrossRef](#)]
20. Sharma, S.K.; Chiang, L.Y.; Hamblin, M.R. Photodynamic Therapy with Fullerenes in Vivo: Reality or a Dream? *Nanomedicine* **2011**, *6*, 1813–1825. [[CrossRef](#)]
21. Simon, H.-U.; Haj-Yehia, A.; Levi-Schaffer, F. Role of Reactive Oxygen Species (ROS) in Apoptosis Induction. *Apoptosis* **2000**, *5*, 415–418. [[CrossRef](#)]
22. Matés, J.M.; Sánchez-Jiménez, F.M. Role of Reactive Oxygen Species in Apoptosis: Implications for Cancer Therapy. *Int. J. Biochem. Cell Biol.* **2000**, *32*, 157–170. [[CrossRef](#)] [[PubMed](#)]
23. Pelicano, H.; Carney, D.; Huang, P. ROS Stress in Cancer Cells and Therapeutic Implications. *Drug Resist. Updates* **2004**, *7*, 97–110. [[CrossRef](#)] [[PubMed](#)]
24. Mittler, R. ROS Are Good. *Trends Plant Sci.* **2017**, *22*, 11–19. [[CrossRef](#)] [[PubMed](#)]
25. Yumita, N.; Nishigaki, R.; Umemura, K.; Umemura, S. Hematoporphyrin as a Sensitizer of Cell-Damaging Effect of Ultrasound. *Jpn. J. Cancer Res.* **1989**, *80*, 219–222. [[CrossRef](#)] [[PubMed](#)]
26. Jeffers, J.; Feng, R.Q.; Fowlkes, J.B.; Brenner, D.E.; Cain, C.A. Sonodynamic Therapy: Activation of Anticancer Agents with Ultrasound. In Proceedings of the IEEE 1991 Ultrasonics Symposium, Orlando, FL, USA, 8–11 December 1991; Volume 2, pp. 1367–1370.
27. Bosca, F.; Corazzari, I.; Foglietta, F.; Canaparo, R.; Durando, G.; Pastero, L.; Arpicco, S.; Dosio, F.; Zonari, D.; Cravotto, G.; et al. SWCNT-Porphyrin Nano-Hybrids Selectively Activated by Ultrasound: An Interesting Model for Sonodynamic Applications. *RSC Adv.* **2020**, *10*, 21736–21744. [[CrossRef](#)] [[PubMed](#)]
28. Son, S.; Kim, J.H.; Wang, X.; Zhang, C.; Yoon, S.A.; Shin, J.; Sharma, A.; Lee, M.H.; Cheng, L.; Wu, J.; et al. Multifunctional Sonosensitizers in Sonodynamic Cancer Therapy. *Chem. Soc. Rev.* **2020**, *49*, 3244–3261. [[CrossRef](#)] [[PubMed](#)]
29. Tsuru, H.; Shibaguchi, H.; Kuroki, M.; Yamashita, Y.; Kuroki, M. Tumor Growth Inhibition by Sonodynamic Therapy Using a Novel Sonosensitizer. *Free Radic. Biol. Med.* **2012**, *53*, 464–472. [[CrossRef](#)] [[PubMed](#)]
30. Gorgizadeh, M.; Azarpira, N.; Lotfi, M.; Daneshvar, F.; Salehi, F.; Sattarahmady, N. Sonodynamic Cancer Therapy by a Nickel Ferrite/Carbon Nanocomposite on Melanoma Tumor: In Vitro and in Vivo Studies. *Photodiagnosis Photodyn. Ther.* **2019**, *27*, 27–33. [[CrossRef](#)]
31. Yamaguchi, S.; Kobayashi, H.; Narita, T.; Kanehira, K.; Sonezaki, S.; Kudo, N.; Kubota, Y.; Terasaka, S.; Houkin, K. Sonodynamic Therapy Using Water-Dispersed TiO₂-Polyethylene Glycol Compound on Glioma Cells: Comparison of Cytotoxic Mechanism with Photodynamic Therapy. *Ultrason. Sonochem.* **2011**, *18*, 1197–1204. [[CrossRef](#)]
32. Yang, C.-C.; Wang, C.-X.; Kuan, C.-Y.; Chi, C.-Y.; Chen, C.-Y.; Lin, Y.-Y.; Chen, G.-S.; Hou, C.-H.; Lin, F.-H. Using C-Doped TiO₂ Nanoparticles as a Novel Sonosensitizer for Cancer Treatment. *Antioxidants* **2020**, *9*, 880. [[CrossRef](#)]
33. Behzadpour, N.; Ranjbar, A.; Azarpira, N.; Sattarahmady, N. Development of a Composite of Polypyrrole-Coated Carbon Nanotubes as a Sonosensitizer for Treatment of Melanoma Cancer Under Multi-Step Ultrasound Irradiation. *Ultrasound Med. Biol.* **2020**, *46*, 2322–2334. [[CrossRef](#)] [[PubMed](#)]
34. Wang, C.-J.; Li, W. Preparation and Sonodynamic Antitumor Effect of Protohemin-Conjugated Multiwalled Carbon Nanotubes Functionalized with Carboxylic Group. *Drug Dev. Res.* **2016**, *77*, 152–158. [[CrossRef](#)] [[PubMed](#)]
35. Lee, H.R.; Kim, D.W.; Jones, V.O.; Choi, Y.; Ferry, V.E.; Geller, M.A.; Azarin, S.M. Sonosensitizer-Functionalized Graphene Nanoribbons for Adhesion Blocking and Sonodynamic Ablation of Ovarian Cancer Spheroids. *Adv. Healthc. Mater.* **2021**, *10*, e2001368. [[CrossRef](#)] [[PubMed](#)]
36. Radivoievych, A.; Kolp, B.; Grebinyk, S.; Prylutska, S.; Ritter, U.; Zolk, O.; Glöckler, J.; Frohme, M.; Grebinyk, A. Silent Death by Sound: C₆₀ Fullerene Sonodynamic Treatment of Cancer Cells. *Int. J. Mol. Sci.* **2023**, *24*, 1020. [[CrossRef](#)] [[PubMed](#)]
37. Yumita, N.; Watanabe, T.; Chen, F.-S.; Momose, Y.; Umemura, S.-I. Induction of Apoptosis by Functionalized Fullerene-Based Sonodynamic Therapy in HL-60 Cells. *Anticancer Res.* **2016**, *36*, 2665–2674. [[PubMed](#)]
38. Yumita, N.; Iwase, Y.; Imaizumi, T.; Sakurazawa, A.; Kaya, Y.; Nishi, K.; Ikeda, T.; Umemura, S.-I.; Chen, F.-S.; Momose, Y. Sonodynamically-Induced Anticancer Effects by Functionalized Fullerenes. *Anticancer Res.* **2013**, *33*, 3145–3151. [[PubMed](#)]
39. Liu, Y.; Li, Z.; Fan, F.; Zhu, X.; Jia, L.; Chen, M.; Du, P.; Yang, L.; Yang, S. Boosting Antitumor Sonodynamic Therapy Efficacy of Black Phosphorus via Covalent Functionalization. *Adv. Sci.* **2021**, *8*, e2102422. [[CrossRef](#)] [[PubMed](#)]
40. Pal, S.L.; Jana, U.; Manna, P.K.; Mohanta, G.P.; Manavalan, R. Nanoparticle: An Overview of Preparation and Characterization. *J. Appl. Pharm. Sci.* **2011**, *1*, 228–234.
41. Hensel, K.; Mienkina, M.P.; Schmitz, G. Analysis of Ultrasound Fields in Cell Culture Wells for In Vitro Ultrasound Therapy Experiments. *Ultrasound Med. Biol.* **2011**, *37*, 2105–2115. [[CrossRef](#)]
42. Araújo Martins, Y.; Zeferino Pavan, T.; Fonseca Vianna Lopez, R. Sonodynamic Therapy: Ultrasound Parameters and in Vitro Experimental Configurations. *Int. J. Pharm.* **2021**, *610*, 121243. [[CrossRef](#)]
43. Grebinyk, A.; Prylutska, S.; Grebinyk, S.; Evstigneev, M.; Krysiuk, I.; Skaterna, T.; Horak, I.; Sun, Y.; Drobot, L.; Matyshevska, O.; et al. Antitumor Efficiency of the Natural Alkaloid Berberine Complexed with C₆₀ Fullerene in Lewis Lung Carcinoma in Vitro and in Vivo. *Cancer Nanotechnol. Basic Transl. Clin. Res.* **2021**, *12*, 24. [[CrossRef](#)]
44. Liu, H.; Zheng, T.; Zhou, Z.; Hu, A.; Li, M.; Zhang, Z.; Yu, G.; Feng, H.; An, Y.; Peng, J.; et al. Berberine Nanoparticles for Promising Sonodynamic Therapy of a HeLa Xenograft Tumour. *RSC Adv.* **2019**, *9*, 10528–10535. [[CrossRef](#)] [[PubMed](#)]

45. Geng, C.; Zhang, Y.; Hidru, T.H.; Zhi, L.; Tao, M.; Zou, L.; Chen, C.; Li, H.; Liu, Y. Sonodynamic Therapy: A Potential Treatment for Atherosclerosis. *Life Sci.* **2018**, *207*, 304–313. [[CrossRef](#)] [[PubMed](#)]
46. Guamán Ortiz, L.M.; Lombardi, P.; Tillhon, M.; Scovassi, A.I. Berberine, an Epiphany Against Cancer. *Molecules* **2014**, *19*, 12349–12367. [[CrossRef](#)] [[PubMed](#)]
47. Prylutska, S.V.; Grynyuk, I.I.; Grebinyk, S.M.; Matyshevskaya, O.P.; Prylutskiy, Y.I.; Ritter, U.; Siegmund, C.; Scharff, P. Comparative Study of Biological Action of Fullerenes C₆₀ and Carbon Nanotubes in Thymus Cells. *Mat.-Wiss. U. Werkstofftech.* **2009**, *40*, 238–241. [[CrossRef](#)]
48. Prylutska, S.V.; Matyshevskaya, O.P.; Golub, A.A.; Prylutskiy, Y.I.; Potebnya, G.P.; Ritter, U.; Scharff, P. Study of C₆₀ Fullerenes and C₆₀-Containing Composites Cytotoxicity in Vitro. *Mater. Sci. Eng. C* **2007**, *27*, 1121–1124. [[CrossRef](#)]
49. Grebinyk, A.; Grebinyk, S.; Prylutska, S.; Ritter, U.; Matyshevskaya, O.; Dandekar, T.; Frohme, M. C₆₀ Fullerene Accumulation in Human Leukemic Cells and Perspectives of LED-Mediated Photodynamic Therapy. *Free Radic. Biol. Med.* **2018**, *124*, 319–327. [[CrossRef](#)]
50. Grebinyk, A.; Prylutska, S.; Chepurina, O.; Grebinyk, S.; Prylutskiy, Y.; Ritter, U.; Ohulchanskiy, T.Y.; Matyshevskaya, O.; Dandekar, T.; Frohme, M. Synergy of Chemo- and Photodynamic Therapies with C₆₀ Fullerene-Doxorubicin Nanocomplex. *Nanomaterials* **2019**, *9*, 1540. [[CrossRef](#)]
51. Grebinyk, S.M.; Palyvoda, K.O.; Prylutska, S.V.; Grynyuk, I.I.; Samoilenko, A.A.; Drobot, L.B.; Matyshevskaya, O.P. Photoactivated Fullerene C₆₀ Induces Store-Operated Ca²⁺ Entry and Cytochrome c Release in Jurkat Cells. *Ukr. Biokhimičeskii Zhurnal* **2012**, *84*, 58–63.
52. Prylutska, S.V.; Grynyuk, I.I.; Palyvoda, K.O.; Matyshevskaya, O.P. Photoinduced Cytotoxic Effect of Fullerenes C₆₀ on Transformed T-Lymphocytes. *Exp. Oncol.* **2010**, *32*, 29–32.
53. Scharff, P.; Risch, K.; Carta-Abelmann, L.; Dmytruk, I.M.; Bilyi, M.M.; Golub, A.; Khavryuchenko, A.V.; Buzaneva, E.; Aksenov, V.; Avdeev, M.V.; et al. Structure of C₆₀ Fullerene in Water: Spectroscopic Data. *Carbon* **2004**, *42*, 1203–1206. [[CrossRef](#)]
54. Liu, L.; Yang, Y.; Liu, P.; Tan, W. The Influence of Air Content in Water on Ultrasonic Cavitation Field. *Ultrason. Sonochem.* **2014**, *21*, 566–571. [[CrossRef](#)] [[PubMed](#)]
55. Carmichael, J.; DeGraff, W.G.; Gazdar, A.F.; Minna, J.D.; Mitchell, J.B. Evaluation of a Tetrazolium-Based Semiautomated Colorimetric Assay: Assessment of Chemosensitivity Testing. *Cancer Res.* **1987**, *47*, 936–942. [[PubMed](#)]
56. Didenko, Y.T.; Gordeychuk, T.V.; Koretz, V.L. The Effect of Ultrasound Power on Water Sonoluminescence. *J. Sound Vib.* **1991**, *147*, 409–416. [[CrossRef](#)]
57. Putterman, S.J.; Weninger, K.R. Sonoluminescence: How Bubbles Turn Sound into Light. *Annu. Rev. Fluid Mech.* **2000**, *32*, 445–476. [[CrossRef](#)]
58. Suslick, K.S.; Flannigan, D.J. Inside a Collapsing Bubble: Sonoluminescence and the Conditions During Cavitation. *Annu. Rev. Phys. Chem.* **2008**, *59*, 659–683. [[CrossRef](#)] [[PubMed](#)]
59. Secomski, W.; Bilmin, K.; Kujawska, T.; Nowicki, A.; Grieb, P.; Lewin, P.A. In Vitro Ultrasound Experiments: Standing Wave and Multiple Reflections Influence on the Outcome. *Ultrasonics* **2017**, *77*, 203–213. [[CrossRef](#)] [[PubMed](#)]
60. Leskinen, J.J.; Hynynen, K. Study of Factors Affecting the Magnitude and Nature of Ultrasound Exposure with In Vitro Set-Ups. *Ultrasound Med. Biol.* **2012**, *38*, 777–794. [[CrossRef](#)]
61. Liu, B.; Xia, H.; Fei, G.; Li, G.; Fan, W. High-Intensity Focused Ultrasound-Induced Thermal Effect for Solid Polymer Materials. *Macromol. Chem. Phys.* **2013**, *214*, 2519–2527. [[CrossRef](#)]
62. O'Brien, W.D. Ultrasound–Biophysics Mechanisms. *Prog. Biophys. Mol. Biol.* **2007**, *93*, 212–255. [[CrossRef](#)]
63. Leung, K.S.; Cheung, W.H.; Zhang, C.; Lee, K.M.; Lo, H.K. Low Intensity Pulsed Ultrasound Stimulates Osteogenic Activity of Human Periosteal Cells. *Clin. Orthop. Relat. Res.* **2004**, *418*, 253–259. [[CrossRef](#)] [[PubMed](#)]
64. Puts, R.; Ruschke, K.; Kadow-Romacker, A.; Hwang, S.; Jenderka, K.-V.; Knaus, P.; Raum, K. Mechanosensitive Response of Murine C2C12 Myoblasts to Focused Low-Intensity Pulsed Ultrasound (FLIPUS) Stimulation. In Proceedings of the 2015 6th European Symposium on Ultrasonic Characterization of Bone, Corfu, Greece, 10–12 June 2015; pp. 1–4.
65. Nomikou, N.; Sterrett, C.; Arthur, C.; McCaughan, B.; Callan, J.F.; McHale, A.P. The Effects of Ultrasound and Light on Indocyanine-Green-Treated Tumour Cells and Tissues. *ChemMedChem* **2012**, *7*, 1465–1471. [[CrossRef](#)] [[PubMed](#)]
66. Masters, J.R. HeLa Cells 50 Years on: The Good, the Bad and the Ugly. *Nat. Rev. Cancer* **2002**, *2*, 315–319. [[CrossRef](#)] [[PubMed](#)]
67. Cho, H.-Y.; Reddy, S.P.; Kleeberger, S.R. Nrf2 Defends the Lung from Oxidative Stress. *Antioxid. Redox Signal.* **2006**, *8*, 76–87. [[CrossRef](#)] [[PubMed](#)]
68. Adinolfi, S.; Patinen, T.; Jawahar Deen, A.; Pitkänen, S.; Härkönen, J.; Kansanen, E.; Küblbeck, J.; Levonen, A.-L. The KEAP1-NRF2 Pathway: Targets for Therapy and Role in Cancer. *Redox Biol.* **2023**, *63*, 102726. [[CrossRef](#)] [[PubMed](#)]
69. Sudha, A.; Bhati, D.; Dhankhar, N. A Comprehensive Review of the Many Models Used In Lung Cancer Research. *Int. J. Pharm. Res. Appl.* **2022**, *7*, 509–517.
70. Lin, Y.-L.; Li, Y. Study on the Hepatocellular Carcinoma Model with Metastasis. *Genes Dis.* **2020**, *7*, 336–350. [[CrossRef](#)] [[PubMed](#)]
71. Kudo, N.; Miyaoka, T.; Okada, K.; Yamamoto, K.; Niwa, K. Study on Mechanism of Cell Damage Caused by Microbubbles Exposed to Ultrasound. In Proceedings of the 2002 IEEE Ultrasonics Symposium, 2002, Munich, Germany, 8–11 October 2002; Volume 2, pp. 1383–1386.
72. Ellwart, J.W.; Brettel, H.; Kober, L.O. Cell Membrane Damage by Ultrasound at Different Cell Concentrations. *Ultrasound Med. Biol.* **1988**, *14*, 43–50. [[CrossRef](#)]

73. Didenko, Y.T.; Gordeychuk, T.V. Multibubble Sonoluminescence Spectra of Water Which Resemble Single-Bubble Sonoluminescence. *Phys. Rev. Lett.* **2000**, *84*, 5640–5643. [[CrossRef](#)]
74. Matula, T.J.; Roy, R.A.; Mourad, P.D.; McNamara, W.B., III; Suslick, K.S. Comparison of Multibubble and Single-Bubble Sonoluminescence Spectra. *Phys. Rev. Lett.* **1995**, *75*, 2602–2605. [[CrossRef](#)]
75. Susana Diaz, M.; Liliana Freile, M.; Isela Gutiérrez, M. Solvent Effect on the UV/Vis Absorption and Fluorescence Spectroscopic Properties of Berberine. *Photochem. Photobiol. Sci.* **2009**, *8*, 970–974. [[CrossRef](#)] [[PubMed](#)]
76. Wang, H.; Liu, X.; Yan, X.; Fan, J.; Li, D.; Ren, J.; Qu, X. A MXene-Derived Redox Homeostasis Regulator Perturbs the Nrf2 Antioxidant Program for Reinforced Sonodynamic Therapy. *Chem. Sci.* **2022**, *13*, 6704–6714. [[CrossRef](#)] [[PubMed](#)]
77. Ketelut-Carneiro, N.; Fitzgerald, K.A. Apoptosis, Pyroptosis, and Necroptosis—Oh My! The Many Ways a Cell Can Die. *J. Mol. Biol.* **2022**, *434*, 167378. [[CrossRef](#)] [[PubMed](#)]
78. Duprez, L.; Wirawan, E.; Berghe, T.V.; Vandenabeele, P. Major Cell Death Pathways at a Glance. *Microbes Infect.* **2009**, *11*, 1050–1062. [[CrossRef](#)] [[PubMed](#)]
79. Tolkachov, M.; Sokolova, V.; Loza, K.; Korolovych, V.; Prylutsky, Y.; Epple, M.; Ritter, U.; Scharff, P. Study of Biocompatibility Effect of Nanocarbon Particles on Various Cell Types in Vitro: Untersuchungen Zur Biokompatibilität von Kohlenstoff-Nanoröhren Auf Verschiedenen Zelltypen in Vitro. *Mat. Wiss. U. Werkst.* **2016**, *47*, 216–221. [[CrossRef](#)]
80. Prylutska, S.V.; Grebinyk, A.G.; Lynchak, O.V.; Byelinska, I.V.; Cherepanov, V.V.; Tauscher, E.; Matyshevska, O.P.; Prylutsky, Y.I.; Rybalchenko, V.K.; Ritter, U.; et al. *In Vitro* and *in Vivo* Toxicity of Pristine C₆₀ Fullerene Aqueous Colloid Solution. *Fuller. Nanotub. Carbon Nanostruct.* **2019**, *27*, 715–728. [[CrossRef](#)]
81. Levi, N.; Hantgan, R.R.; Lively, M.O.; Carroll, D.L.; Prasad, G.L. C₆₀-Fullerenes: Detection of Intracellular Photoluminescence and Lack of Cytotoxic Effects. *J. Nanobiotechnol.* **2006**, *4*, 14. [[CrossRef](#)]
82. Larner, S.F.; Wang, J.; Goodman, J.; O'Donoghue Altman, M.B.; Xin, M.; Wang, K.K.W. In Vitro Neurotoxicity Resulting from Exposure of Cultured Neural Cells to Several Types of Nanoparticles. *J. Cell Death* **2017**, *10*, 1179670717694523. [[CrossRef](#)]
83. Scrivens, W.A.; Tour, J.M.; Creek, K.E.; Pirisi, L. Synthesis of ¹⁴C-Labeled C₆₀, Its Suspension in Water, and Its Uptake by Human Keratinocytes. Available online: <https://pubs.acs.org/doi/pdf/10.1021/ja00089a067> (accessed on 15 December 2022).
84. Liu, S.; Liu, H.; Yin, Z.; Guo, K.; Gao, X. Cytotoxicity of Pristine C₆₀ Fullerene on Baby Hamster Kidney Cells in Solution. *J. Biomater. Nanobiotechnol.* **2012**, *3*, 20590. [[CrossRef](#)]
85. Kheir, M.M.; Wang, Y.; Hua, L.; Hu, J.; Li, L.; Lei, F.; Du, L. Acute Toxicity of Berberine and Its Correlation with the Blood Concentration in Mice. *Food Chem. Toxicol.* **2010**, *48*, 1105–1110. [[CrossRef](#)]
86. Rad, S.Z.K.; Rameshrad, M.; Hosseinzadeh, H. Toxicology Effects of Berberis Vulgaris (Barberry) and Its Active Constituent, Berberine: A Review. *Iran. J. Basic Med. Sci.* **2017**, *20*, 516–529. [[CrossRef](#)]
87. Lagneaux, L.; de Meulenaer, E.C.; Delforge, A.; Dejeneffe, M.; Massy, M.; Moerman, C.; Hannecart, B.; Canivet, Y.; Lepeltier, M.-F.; Bron, D. Ultrasonic Low-Energy Treatment: A Novel Approach to Induce Apoptosis in Human Leukemic Cells. *Exp. Hematol.* **2002**, *30*, 1293–1301. [[CrossRef](#)]
88. Schuster, A.; Schwab, T.; Bischof, M.; Klotz, M.; Lemor, R.; Degel, C.; Schäfer, K.-H. Cell Specific Ultrasound Effects Are Dose and Frequency Dependent. *Ann. Anat. Anat. Anz.* **2013**, *195*, 57–67. [[CrossRef](#)]
89. Ohmura, T.; Fukushima, T.; Shibaguchi, H.; Yoshizawa, S.; Inoue, T.; Kuroki, M.; Sasaki, K.; Umemura, S.-I. Sonodynamic Therapy with 5-Aminolevulinic Acid and Focused Ultrasound for Deep-Seated Intracranial Glioma in Rat. *Anticancer Res.* **2011**, *31*, 2527–2533.
90. Foglietta, F.; Pinnelli, V.; Giuntini, F.; Barbero, N.; Panzanelli, P.; Durando, G.; Terreno, E.; Serpe, L.; Canaparo, R. Sonodynamic Treatment Induces Selective Killing of Cancer Cells in an In Vitro Co-Culture Model. *Cancers* **2021**, *13*, 3852. [[CrossRef](#)] [[PubMed](#)]

Disclaimer/Publisher's Note: The statements, opinions and data contained in all publications are solely those of the individual author(s) and contributor(s) and not of MDPI and/or the editor(s). MDPI and/or the editor(s) disclaim responsibility for any injury to people or property resulting from any ideas, methods, instructions or products referred to in the content.